Developmental Biology **241,** 59–78 (2002)
doi:10.1006/dbio.2001.0494, available online at http://www.idealibrary.com on IDEAL®

Pathways in Regulating Cell Fates in the Zebrafish Gastrula

V. Willot,*,[1] J. Mathieu,*,[1] Yan Lu,* B. Schmid,† S. Sidi,† Yi-Lin Yan,‡ J. H. Postlethwait,‡ M. Mullins,§ F. Rosa,* and N. Peyriéras*,[2]

**U 368 INSERM, Ecole Normale Supérieure, 46 rue d'Ulm, 75005 Paris, France; †Max-Planck-Institut fur Entwicklungsbiologie, Abteilung III, Spemannstrasse 35, Tübingen, D-72076, Germany; ‡Institute of Neuroscience, 1254 University of Oregon, Eugene, Oregon 97403-1254; and §Department of Cell and Developmental Biology, University of Pennsylvania, 421 Curie Boulevard, Philadelphia, Pennsylvania 19104-6058*

It was shown in *Xenopus* and chick that Spemann's organizer activity is regulated through the negative action of Anti-Dorsalizing Morphogenetic Protein (ADMP). We report the characterization and functional properties of *admp* in zebrafish. *admp* expression profile is consistent with a role in the organizer, including the tail organizer. We studied *admp* function through overexpression experiments, with the use of a dominant-negative form (TR-ADMP) and of an antisense morpholino-modified oligonucleotide. Our results indicate that the ADMP pathway causes the restriction of anterior and axial fates and that ADMP, BMP2b, and BMP7 pathways have distinct actions but cooperate in establishing proper dorso-ventral regionalization. This is shown by partial rescue of the dorsalized mutant *snailhouse* and of the ventralized mutant *chordino*, upon *admp* and *tr-admp* RNA injection, respectively. Moreover, ADMP and BMP7 probably form heterodimers as shown by the ability of TR-ADMP and BMP7 to antagonize each other. We observed that a MYC-tagged ADMP was secreted and detected in the extracellular space, suggesting that *admp* could act at a distance. Simultaneous local inhibition of *bmp* function at the blastoderm margin and impairment of ADMP secretion led to the induction of secondary head structures, confirming that the two pathways cooperatively regulate organizer formation and activity.

Key Words: **zebrafish; ADMP; BMP; Spemann organizer.**

INTRODUCTION

The Spemann organizer is a characteristic feature of chordate embryos. It was first defined in grafting experiments through its ability to promote the formation of an ectopic secondary embryonic axis in amphibian embryos (Spemann, 1924). Similarly, an axis duplication assay was used to dissect the molecular mechanisms leading to organizer formation in *Xenopus* (Harland and Gerhart, 1997) and in zebrafish. The zebrafish model system, allowing mutational analyses, lately has become a key model for the understanding of organizer function and axis formation (Kodjabachian *et al.*, 1999; Schier and Talbot, 1998).

In frog and fish embryos, organizer formation is initiated by the nuclear accumulation of β-CATENIN in dorsal blastomeres, under the control of maternal factors (Kelly *et al.*, 2000; Schneider *et al.*, 1996). In overexpression experiments, β-CATENIN is able to promote axis duplications in *Xenopus* (Funayama *et al.*, 1995; Guger and Gumbiner, 1995) and in zebrafish (Kelly *et al.*, 1995). β-CATENIN activates the expression of NODAL signals belonging to the TGF-β superfamily, controlling endoderm and mesoderm formation (Schier and Shen, 2000). In zebrafish, the type I receptor kinase TARAM-A is likely to transduce ACTIVIN/NODAL signals (Thisse and Thisse, 1999; Peyrieras *et al.*, 1998; Renucci *et al.*, 1996). Consistent with this idea, TAR*, a constitutively active form of TARAM-A, induces secondary axial structures (Peyrieras *et al.*, 1996; Renucci *et al.*, 1996).

It was shown in zebrafish that organizer formation requires the repression of the ventralizing bone morphoge-

[1] V.W. and J.M. contributed equally to this work.

[2] To whom correspondence should be addressed. Fax: 33 1 44 32 39 88. E-mail: peyriera@wotan.ens.fr.

0012-1606/01 $35.00

netic protein (BMP) expression and activity (Gonzalez *et al.*, 2000). The transcription factor BOZ/DHARMA acts downstream of the β-CATENIN pathway and represses *bmp2b* expression on the dorsal side of the embryo (Fekany *et al.*, 1999; Koos and Ho, 1999; Yamanaka *et al.*, 1998). Moreover, BMP ventralizing activity is down-regulated through the binding of factors like CHORDIN and NOGGIN, secreted on the dorsal side of the embryo (Piccolo *et al.*, 1996; Zimmerman *et al.*, 1996).

Recently, signals expressed on the dorsal side of the embryo and negatively regulating organizer formation were characterized (Bisgrove *et al.*, 1999; Thisse and Thisse, 1999). This suggests that organizer is induced, maintained, and restricted through a complex network of dorsal positive and negative signals. Anti-dorsalizing morphogenetic protein (ADMP), a member of the BMP family, was characterized in *Xenopus* and chick. ADMP has a typical TGF-β structure (Massagué, 1998). ADMP is proposed to antagonize organizer formation or to regionalize the organizer by inhibiting head formation and promoting trunk formation (Dosch and Niehrs, 2000; Joubin and Stern, 1999; Moos *et al.*, 1995).

In this study, we characterized zebrafish *admp* in order to document its role in the zebrafish model system. We approached ADMP function through overexpression experiments and the use of a truncated form, TR-ADMP, with dominant-negative activity. The phenotypic effect of ADMP is reminiscent of the ventralizing BMP activity. However, our results lead us to conclude that ADMP, BMP2b, and BMP7 have distinct phenotypic effects. ADMP inhibits axial structures, while BMP7 primarily antagonizes anterior fates and BMP2b is more potent in promoting the expansion of ventral fates. We hypothesize that ADMP function is part of organizer activity and is involved in head, trunk, and tail formation. ADMP also acts on dorso-ventral regionalization and cooperates with the BMP-mediated pathway in regulating cell fates in the zebrafish gastrula through: (1) the restriction of anterior and axial fates and (2) the formation of heterodimers as suggested by TR-ADMP and BMP7 antagonistic effects.

MATERIALS AND METHODS

Fish strains. Wild-type embryos from West Aquarium (Bad Lauterbach, Germany) were kept in closed stocks and inbred for at least five generations. The following mutant strains were used : *bozozok* (*m168* allele) (Fekany *et al.*, 1999), MZoep (*tz57* allele) (Gritsman *et al.*, 1999), *piggytail* (*dty40* allele), *snailhouse* (*ty68a* allele), *chordino* (*at50* allele), and *swirl* (*ta72* allele) (Hammerschmidt *et al.*, 1996a; Mullins *et al.*, 1996).

admp cloning. An *admp* DNA fragment was obtained by PCR from a gastrula-stage cDNA library (M. Rebagliati and I. Dawid) with the following degenerate primers derived from the *Xenopus* ADMP sequence: forward, ATH GGI TGG WSN GGI TGG ATH AT; reverse, AT ISW YTG NAC NGT IGC RTG RTT. The resulting 121-bp fragment was cloned in a PCR II vector by using a TA cloning kit (Invitrogen) and used as a probe to screen the same cDNA library. Thirteen independent cDNAs were obtained and sequenced. A full-length cDNA (1649 bp) was subcloned into plasmids pBS SK− and pSP64T. TR-ADMP, a truncated form of ADMP, is deleted of the last 113 amino acids, i.e., the entire mature region. A MYC-tagged ADMP was constructed by PCR. The MYC sequence QKLISEEDL was inserted five amino acids downstream of the potential cleavage site (RSPR). C*-ADMP has a mutated cleavage site: HHGPG instead of RRSPR.

bmp2b subcloning. Zebrafish *bmp2b* cDNA was kindly provided by N. Ueno (Nikaido *et al.*, 1997). The *bmp2b* coding sequence was subcloned into pSP64T plasmid. We constructed a truncated form of *bmp2b* (*tr-bmp2b*) deleted of the last 44 amino acids.

Capped RNA and injection. Plasmids were linearized and transcribed *in vitro* by using the SP6 mMessage mMachine transcription kit from Ambion. Injections were performed as described by Wittbrodt and Rosa (1994). Injections at the 16-cell stage were performed as previously described (Peyrieras *et al.*, 1996), with the addition of *nls-gfp* RNA (50 pg) or 2Mda dextran rhodamine (1 ng) (Sigma).

Morpholino injection. An *admp* antisense morpholino-modified oligonuleotide 5′-CAAAGAACATTGCAGACAACATGAT-3′ (Gene Tools, LLC) (sequence complimentary to the predicted start codon is underlined) was prepared as described (Nasevicius and Ekker, 2000) and injected at the one-cell stage (250 or 500 μM) in 1× Danieau solution. The following morpholino, 5′-CCTCTTACCTCAGTTACAATTTATA-3′, had no effect when injected at the same concentration and was used as a negative control.

In vitro translation. *admp* RNA (1 μg) was translated *in vitro* by using a rabbit reticulocyte lysate system (Promega) in the absence or in the presence of morpholino-modified antisense oligonucleotide (10, 2, or 0.4 μg in a reaction volume of 25 μl). The translation products were analyzed by SDS–PAGE on a 12% polyacrylamide gel and detected by autoradiography.

Whole-mount in situ hybridization. Antisense probes were *in vitro* transcribed by using digoxigenin- or fluorescein-labeled UTP (Boehringer). The following probes were used: *admp*, *hgg1* (Thisse *et al.*, 1994), *pax2.1* (Krauss *et al.*, 1991a), *chordino* (Fisher *et al.*, 1997), *fkd3* (Odenthal and Nusslein-Volhard, 1998), *flh* (Talbot *et al.*, 1995), *myoD* (Weinberg *et al.*, 1996), *ntl* (Schulte-Merker *et al.*, 1994), *otx2* (Mori *et al.*, 1994), *her5* (Müller *et al.*, 1996), *fkd6* (Odenthal and Nusslein-Volhard, 1998), *pax6* (Krauss *et al.*, 1991b), and *gata1* (Detrich *et al.*, 1995).Whole-mount staining of embryos was performed as described (Rissi *et al.*, 1995).

Immunocytochemistry. NTL expression was revealed after *in situ* hybridization by using a polyclonal anti-NTL antibody (Schulte-Merker *et al.*, 1994). MYC-ADMP expression was detected following RNA injection at the 16-cell stage (200 pg) together with *nls-gfp* RNA (50 pg). Embryos were fixed at the sphere stage for 6 h in 4% paraformaldehyde and PBS. They were then rinsed in PBS and 0.1% Tween 20 and incubated for 10 min at −20°C in 100% methanol. After a 2-h blocking step in PBS–0.2% gelatin, 0.1% Tween 20, and 5% normal goat serum, they were incubated with an anti-MYC polyclonal antibody (UPSTATE) followed by an anti-rabbit CY5 at a 1000-fold dilution (affinity-purified Fab fragments; Jackson). Embryos freed from their yolk and mounted between a slide and a coverslip separated by a layer of adhesive tape were observed with a confocal microscope (Leica TCS SP2).

RESULTS

Zebrafish admp Cloning and Mapping

We isolated a full-length cDNA encoding the zebrafish anti-dorsalizing morphogenetic protein (ADMP) precursor, using degenerate primers derived from the pro-region of *Xenopus* ADMP (see Materials and Methods). The deduced amino acid sequence shares significant identity with the *Xenopus* (79%) and chick protein (76%) in the mature region (Fig. 1). The ADMP pro-domain is less conserved and shares 64% identity with the *Xenopus* and 56% with the chick protein.

A polymorphism between the C32 and SJD fish strains was used to follow the segregation with mapped markers in the haploid progeny of a C32/SJD female. The *admp* locus mapped to linkage group 2, between markers 3D1800 and 21AE1090 (Postlethwait *et al.*, 1998). The *admp* locus does not correspond to any mutation identified so far.

admp Is Expressed in the Zebrafish Organizer

admp transcripts were undetectable at the eight-cell stage (Fig. 2A). The absence of maternal expression was confirmed by RT-PCR (data not shown). Soon after the midblastula transition, *admp* was expressed asymetrically in the blastoderm (not shown). At the sphere stage, the *admp* expression domain covered much of the blastoderm in a radially asymetric way (Fig. 2B). The signal was stronger in superficial blastomeres (Fig. 2H). Until 50% epiboly, the *admp* expression domain did not reach the margin (Figs. 2B and 2H, and data not shown). At the onset of gastrulation, it encompassed the embryonic shield, the zebrafish organizer, and was epiblastic (Figs. 2C and 2I). As gastrulation proceeded, the expression domain extended along the antero-posterior axis (Fig. 2E). At 80% epiboly, *admp* transcripts were detected in cells involuting at the dorsal margin of the blastoderm (Fig. 2D). In the trunk, a few *ntl*-positive presumptive notochord cells expressed *admp*, but the bulk of expression was found in cells located between the *ntl* expression domain and the yolk syncitial layer (YSL). In the most anterior region, *admp* transcripts were detected in deep cells as well as in the neuroectodermal layer. At the end of gastrulation, *admp* was expressed in three major domains (Figs. 2F, 2G, 2J, 2K, and 2M). Posteriorly, *admp* was expressed in the tail bud and paraxial mesoderm (Figs. 2F and 2J). Posterior to the midbrain–hindbrain boundary, *admp* transcripts were detected close to the YSL, in a position corresponding to the notochord (Fig. 2M). Anteriorly, *admp* was expressed in the prechordal plate posterior to the hatching gland domain (Figs. 2J and 2K). During somitogenesis, the *admp* expression domain was restricted to a small region of the growing tail bud, surrounding the tip of the notochord, and next to the Kupffer's vesicle (Figs. 2L and 2N). The latter is a teleost-specific structure derived from a small population of non-involuting cells, the so-called forerunner cells, that remain located at the margin of the dorsal blastoderm during gastrulation, and then contribute to tail formation (D'Amico and Cooper, 1997). *admp* transcripts were no longer detected after somitogenesis.

admp Overexpression Causes a Loss of Dorsal Fates

The potential role of *admp* during zebrafish development was studied through overexpression experiments. We first injected *admp* RNA or *lacZ* RNA as a control, at the one-cell stage. With 600 pg RNA, embryos observed after 1 day of development displayed a variable loss of dorso-axial structures, falling into three major classes (Fig. 3, and Table 1). Class 1, the weakest phenotype, exhibited notochord disruption in the tail, a shorter axis and slightly smaller head and eyes (Fig. 3B); class 2 showed notochord disruption in the trunk, fused somites and smaller head and eyes (Fig. 3C); class 3 had a complete loss of notochord and strongly reduced head and eyes (Fig. 3D). At a lower dose (100 pg), the same phenotypes were observed, but at lower frequencies (Table 1). Although these morphologies were reminiscent of ventralized phenotypes, they clearly showed distinct features. In class 1 and 2 phenotypes, *admp* overexpression promoted notochord disruption without causing major anterior defects. Even at high doses of *admp* RNA, a complete loss of anterior structures was rarely observed (see class 4 in Table 1). This differs from what was found in *bmp2b* or *bmp4* overexpression experiments where, in weakly ventralized phenotypes (V1), anterior structures were strongly reduced with no notochord disruption (Nguyen *et al.*, 1998; Nikaido *et al.*, 1997). However, the expression domain of the transcription factor *gata1* observed at the 10-somite stage was slightly expanded (Fig. 4E), indicating an excess of ventrally derived tissues as described in ventralized mutant phenotypes (Hammerschmidt *et al.*, 1996a,b; Kishimoto *et al.*, 1997; Nguyen *et al.*, 1998).

The phenotypes obtained 30 h after injection could be correlated with *in situ* hybridization patterns obtained at the beginning of somitogenesis (Figs. 3E and 3F). More than 90% of the injected embryos displayed a partial or complete fusion at the midline of *myoD* expression domains corresponding to the adaxial mesoderm, with disruption of the notochord (*ntl* positive). We observed an antero-posterior gradient in notochord defects, the anterior ones being less frequent and always associated with posterior defects, thus corresponding to the most severe phenotypes. Staining of the hatching gland with *hgg1*, the midbrain–hindbrain boundary with *pax2.1*, and rhombomeres 3 and 5 with *krox 20*, confirmed a slight reduction of anterior structures (Fig. 3F).

The extent of neural defects caused by *admp* overexpression was further studied by *in situ* hybridization at the end of gastrulation and at the 10-somite stage (Fig. 4). Staining of the presumptive forebrain and midbrain with *otx2*, the forebreain with *pax6*, the midbrain–hindbrain boundary with *her5*, rhombomere 3 and 5 with *krox 20*, and neural crest with *fkd6*, indicated that the antero-posterior patterning of the

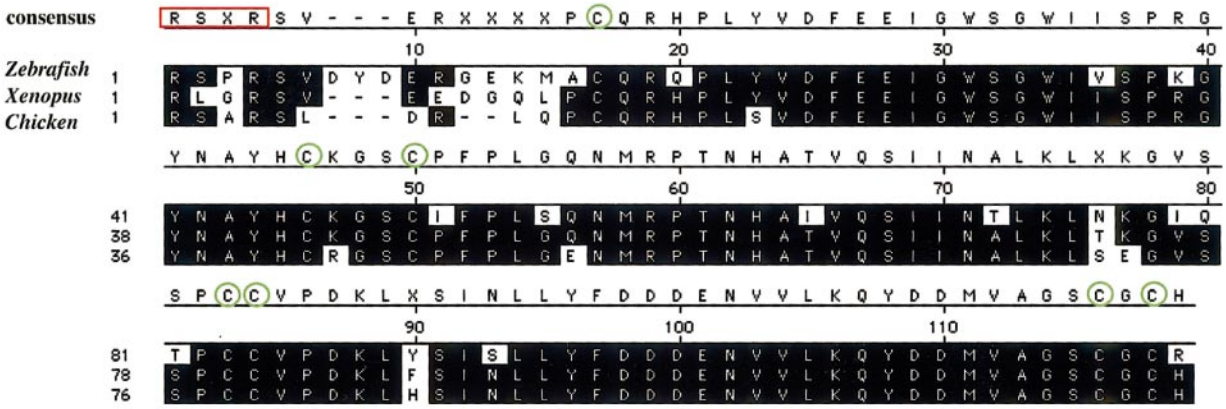

1

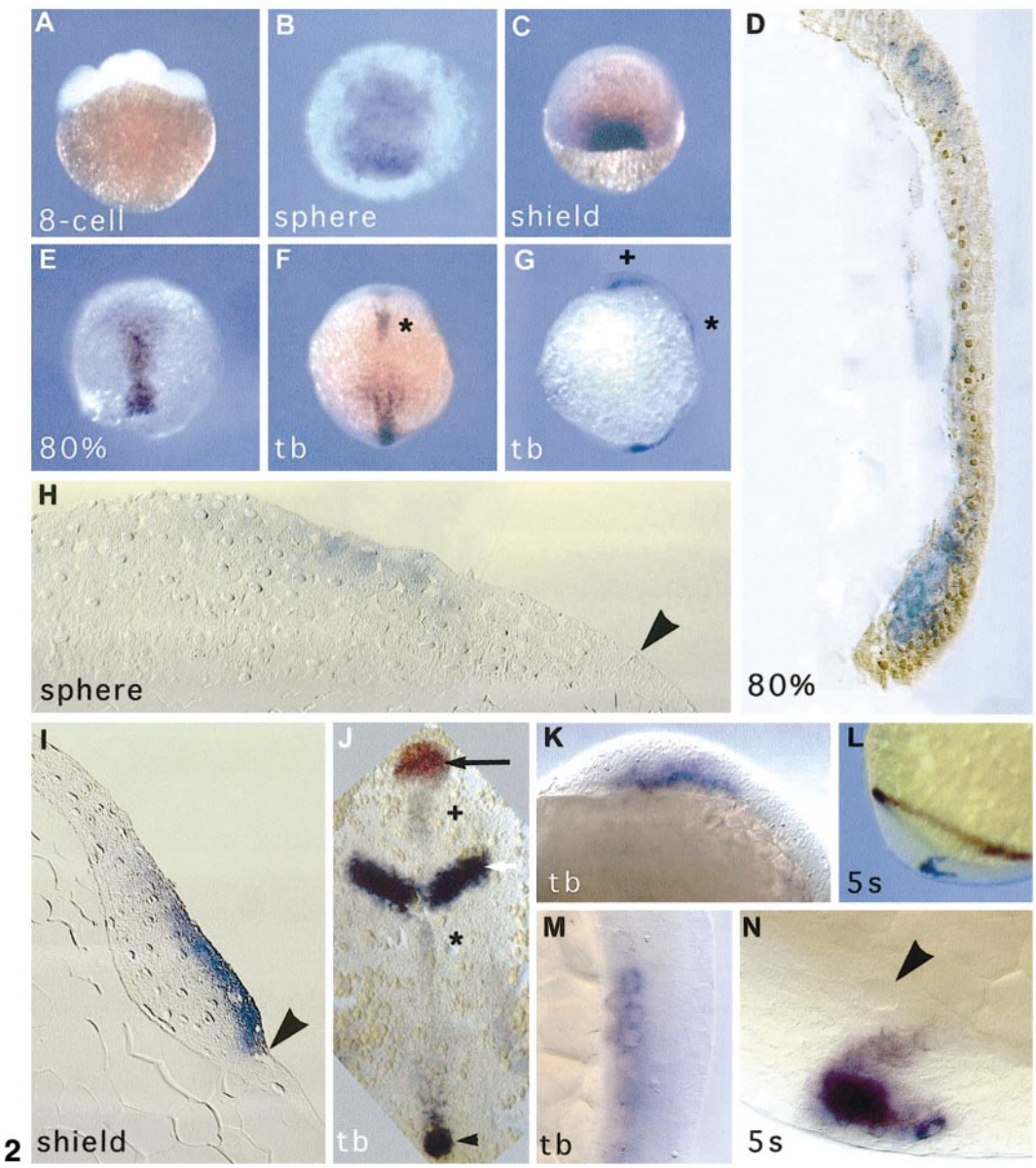

2

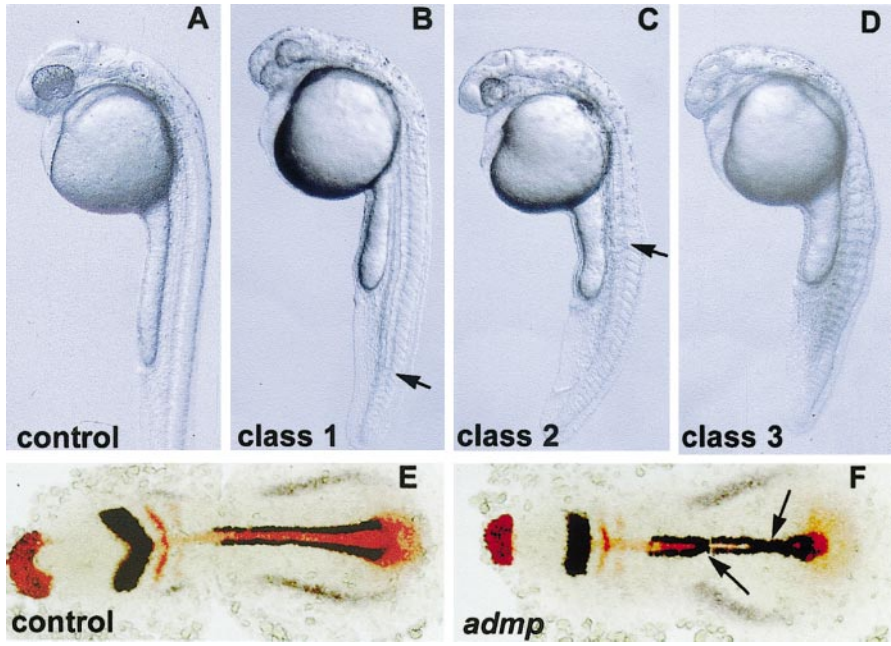

FIG. 3. *admp* overexpression causes the loss of dorsal fates. *wt* embryos were injected at the one-cell stage with *admp* RNA (600 pg) and compared to uninjected siblings (control). (A–D) Live embryos at 1 day of development. (E, F) Flat mounts of embryos stained at the one- to three-somite stage with *myoD* and *pax2.1* in dark blue, *hgg1*, *krox20*, and *ntl* in red; anterior to the left. (A) Uninjected embryo. (B–D) *admp*-injected embryos. (B) Class 1 phenotype. (C) Class 2 phenotype. (D) Class 3 phenotype. (B, C) Arrows indicate the posterior limit of the truncated notochord. (E) Uninjected embryo. (F) *admp*-injected embryo; notochord defects and fusion of *myoD* expression domains at the midline are indicated (arrows).

neural plate was normal. However, at the end of gastrulation, the presumptive forebrain and midbrain territory was reduced (Fig 4B). The expression domain of *pax 6* observed at the 10-somite stage was much smaller, consistent with the eyes reduction observed after 1 day of development (Fig. 4E). *fkd6* staining of the neural crest territory was not affected but revealed a much narrower neural plate (Fig. 4H).

Altogether, our results suggest that ADMP is involved in the restriction of dorso-axial territories along the antero-posterior axis.

MYC-ADMP Is Able to Diffuse throughout the Blastoderm

As other BMPs, the ADMP protein is expected to be secreted after dimerization and cleavage of its precursor form (Massagué, 1998). ADMP might then diffuse to allow the formation of a gradient. In order to investigate ADMP secretion and diffusion, we examined the expression of a tagged form of ADMP. MYC-ADMP is functional and its biological activity is similar to ADMP (Table 1). RNA

FIG. 1. *admp* sequence comparisons. Amino-acid sequences of the mature region of *admp* from zebrafish; *Xenopus* and chick are aligned. The putative cleavage site is outlined by the red box; the seven conserved cysteines are circled in green. *admp* cDNA sequence is available under the accession number AJ315468.

FIG. 2. *admp* expression during early development. *In situ* hybridization was performed with an *admp* antisense probe. (A) No signal is detected at the eight-cell stage. (B) Sphere stage, animal pole view. The *admp* expression domain is radially asymetric. (C) Shield stage, dorsal view, ventral to the top. *admp* RNA is expressed in the embryonic shield. (D) Sagittal section at 80% epiboly, dorsal to the right, animal pole to the top; *admp* RNA expression in blue; NTL protein expression in brown. (E) 80% epiboly, dorsal view. *admp* RNA is expressed along the antero-posterior axis during gastrulation. (F) Tail bud stage, dorsal view. *admp* expression is discontinuous along the midline. (G) Tail bud stage, lateral view. (H) Sagittal section at the sphere stage, dorsal to the right. An arrowhead indicates the blastoderm margin. (I) Sagittal section through the embryonic shield. An arrowhead shows the blastoderm margin. (J) Flat mount at tail bud stage. Black arrow, hatching gland territory, stained in red with an *hgg1* probe; white arrow, midbrain–hindbrain boundary, stained in purple with a *pax2.1* probe; black arrowhead, admp RNA staining in the tailbud. (K) Tailbud stage, lateral view; higher magnification of the region marked (+) in (G) and (J). *admp* RNA is expressed in the prechordal plate. (L) Five-somite stage, lateral view of the tail bud; staining for *pax2.1* and *admp* both in purple. (M) Tailbud stage, lateral view, higher magnification of the region marked (*) in (F, G, J). Axial staining posterior to the midbarin-hindbrain boundary. (N) Five-somite stage; note the Kupffer's vesicle (arrowhead) next to the *admp* staining.

TABLE 1

Phenotypic Effects of *admp, tr-admp, bmp2, tr-bmp2,* and *bmp7* RNA Injections

mRNA	pg	*n*	Class 1	Class 2	Class 3	Class 4	WT	A1	A2	A3	A4	Dead
myc-admp[a]	600	119	6	38	56	0	0					
admp[a]	600	131	18	38	43	1[b]	0					
admp[a]	100	96	30	5	3	0	62					
tr-admp[c]	600	52					6	15	21	31	27	0
tr-admp[c]	300	67					12	20	44	19	2	3
admp +	600											
tr-admp	600	64	11		3	0	20	14	30	5	6	11

mRNA	pg	*n*	V1	V2	V3	V4	WT	C1	C2	C3	C4	Dead or C5
bmp2b[d]	80	95	12	14	41	33						
bmp2b[d]	40	51	31	20	12	12	25					
bmp2b[d]	10	53	23	31	4	2	31					
tr-bmp2b[c]	600	86					19	38	8	16	14	5
bmp2b +	40											
tr-bmp2b	600	43	7	39	0	0	54					
bmp2b +	40			33					45[f]			
tr-admp	600	58		ventralized phenotype			19		ventralized and dorsalized features			3
bmp2b +	80											
admp[g]	100	107				100						
bmp2b +	10											
admp[g]	100	58	4	52	36	1	7					

mRNA	pg	*n*	Type I	Type II	Type III	Type IV	WT	A1	A2	A3	A4	Dead
bmp7[h]	160	121	16	17	17[i]							50
bmp7[h]	40	47	36	37	25	2						
bmp7 +	160											
tr-admp[i]	600	53					20	40	25	9	2	4
bmp7 +	160											
tr-admp[i]	300	62			21			79				
bmp7 +	160											
admp[k]	100	54	20[k]	39[k]	22[k]	17[k]	2[k]					

[a] *admp* or *myc-admp* RNA injected at the one-cell stage gave rise after 1 day of development to the phenotypes shown in Fig. 3.

[b] Embryos devoid of head structures were assigned to class 4.

[c] *tr-admp* RNA gave rise to axialized phenotypes designated A1, 2, 3, and 4 to distinguish them from the dorsalized phenotypes C1–C5.

[d] *bmp2b* RNA injection gave rise to ventralized phenotypes (Kishimoto *et al.,* 1997). V1, anterior neural defects; V2, reduced or absent notochord; V3, little or no head structures; V4, no anterior structures. See also Fig. 7.

[e] *tr-bmp2b* RNA gave rise to dorsalized phenotypes, and the categories previously described (Kishimoto *et al.,* 1997) were adopted to describe the observed morphologies. C1, loss of ventral tail fin; C2, loss of ventral vein; C3, curved tail; C4, embryonic axis curled on top of the yolk; C5, dead after 1 day of development.

[f] See Fig. 7.

[g] The V1–V4 classes were appropriate to describe the observed phenotypes as embryos displayed severe head defects compared to *admp* RNA injection alone.

[h] *bmp7* RNA injection gave rise to phenotypes designated type I, II, III, IV, and V (dead).

[i] Type III + IV.

[j] *bmp7* + *tr-admp* RNA injection gave rise to moderately axialized phenotypes or with lower doses of *tr-admp* RNA, to embryos wild-type looking or showing a reduced head and notochord defects.

[k] *bmp7* + *admp* RNA injection gave rise to ventralized phenotypes best described with the V1–V4 classes.

TABLE 2
Ventral Injection of *myc-admp* RNA

Sorting[a]	0–1[b]	2	3[c]	4	5	6[d]
n	42	21	20	11	16	14
% WT or class 1[e]	45	43	90	82	87	64
% Class 2 or 3[e]	55	57	10	18	13	36

[a] *myc-admp* (300 pg) and *nls-gfp* RNAs (50 pg) were injected at the 16-cell stage into one marginal blastomere. Embryos were sorted at the shield stage according to the position of the injection relative to the dorsal side.
[b] (0–1) Injection close to the dorsal side.
[c] (3) Lateral injection.
[d] (6) Ventral injection.
[e] The phenotypes were observed after 1 day of development and scored as described in Fig. 3.

encoding MYC-ADMP was injected at the 16-cell stage into one marginal blastomere, and the protein was localized by immunocytochemistry at the sphere stage. NLS-GFP was used as a lineage tracer to identify the progeny of the injected cell (Fig. 5). A strong positive signal for MYC was observed both in the cytoplasm and at the periphery of GFP positive cells (Fig. 5A). Thus, the ADMP protein is likely to be secreted. Interestingly, a strong positive signal was also detected at the periphery of GFP-negative cells, indicating a diffusion of MYC-ADMP (Fig. 5A). Protein was detected in most of the blastoderm, suggesting long-range diffusion (Fig. 5C). Consistent with this idea, we observed that injection of *admp* RNA at the 16-cell stage into one marginal blastomere gave rise to a loss of axial structures in the trunk, even when the injected blastomere had a purely ventral fate (position 6 in Table 2). Thus, ectopic ADMP is likely to diffuse from the ventral side throughout the embryo.

ADMP Function Is Impaired by an Antisense Morpholino-Modified Oligonucleotide

After gain-of-function experiments, we approached ADMP function through loss-of-function studies. Morpholinos were described as effective and specific translational inhibitors in zebrafish (Nasevicius and Ekker, 2000). An *admp*-morpholino (Mo) or a control morpholino (Co) was injected at the one-cell stage at a concentration of 250 μM. Mo-injected embryos observed after 1 day of development displayed a shorter embryonic axis and an enlarged trunk. They were devoid of yolk-tube extension but retained the ventral tail fin (Fig. 6B). The morpholino phenotype was rescued by *admp* RNA in a dose-dependent manner (not shown). *In situ* hybridization performed at the three-somite stage on Mo-injected embryos showed a slight expansion of the neural plate revealed by *otx2* and *fkd6* staining and an enlarged notochord, as assessed by the expression of *ntl*, both by *in situ* hybridization (Figs. 6D and 6F) and immunocytochemistry (not shown). The counting of NTL-positive cells in Mo-injected embryos (n = 3; 526 +/− 58) versus uninjected siblings (n = 4; 396 +/− 22) revealed a 20% increase of notochord cells upon Mo injection. Altogether, the morpholino phenotype showed an expansion of dorso-axial structures and was consistent with an *admp* loss-of-function.

We investigated the ability of the *admp*-morpholino (250 and 500 μM) to inhibit the synthesis of a MYC-tagged version of ADMP. RNA encoding MYC-ADMP (50 pg) was injected into one marginal blastomere at the 16-cell stage, together with *nls-gfp* RNA (50 pg), and MYC-ADMP was detected by immunocytochemistry at the sphere stage. The cytoplasmic MYC-positive signal was much weaker in Mo-injected embryos (Fig. 5E) compared to the uninjected ones (Fig. 5D), while the expression of GFP was unaffected. However, some MYC-tagged ADMP was detected in the extracellular space (Fig. 5E). Higher doses of morpholino were used (1 mM) but gave nonspecific effects rendering a more complete inhibition impossible. The ability of the *admp*-morpholino to interfere with ADMP translation in a dose-dependent manner was confirmed *in vitro*, using a rabbit reticulocyte lysate system (Fig. 5).

We conclude from these observations that the *admp*-morpholino specifically inhibited ADMP translation. Mo and *admp* RNA injection had opposite effects. However, the *admp*-morpholino probably only led to a partial loss-of-function.

admp and tr-admp Have Opposite Effects

The morpholino effect was compared with another loss-of-function approach. Like other BMPs, ADMP is likely to act as a cleaved dimer, a property used to generate dominant-negative forms (Wittbrodt and Rosa, 1994). TR-ADMP, devoid of the ADMP mature region, is expected to exhibit such dominant-negative properties. Overexpression of *tr-admp* RNA at the one-cell stage (600 pg) gave rise, at 30 h of development, to phenotypes reminiscent of those described for the dorsalized mutants and classified by Mullins (Mullins *et al.*, 1996). We observed dorsalized-like phenotypes ranging from C1-like to C4-like (Figs. 6G–6I). *tr-admp* promoted an enlargement of the notochord, as assessed by the expression of *ntl*, both by *in situ* hybridization (Fig. 4) and immunocytochemistry (data not shown). *tr-admp* expanded the neural plate as shown by the enlarged expression domain of *otx2*, *her5*, and *krox 20* observed at the end of gastrulation (Fig. 4C) and at the 10-somite stage (Figs. 4F and 4I). At the latter stage, most of the embryos displayed the tail protrusion described for dorsalized phenotypes and a short body axis indicating convergence extension defects (Mullins *et al.*, 1996). *tr-admp* promoted an enlargement of dorso-axial structures at the expanse of the ventral ones as shown by the reduction of *gata1* expression domain at the 10-somite stage (Fig. 4F).

The counting of NTL-positive cells in uninjected (n = 5; 243 cells +/− 25) versus *tr-admp* (n = 5; 376 cells +/−

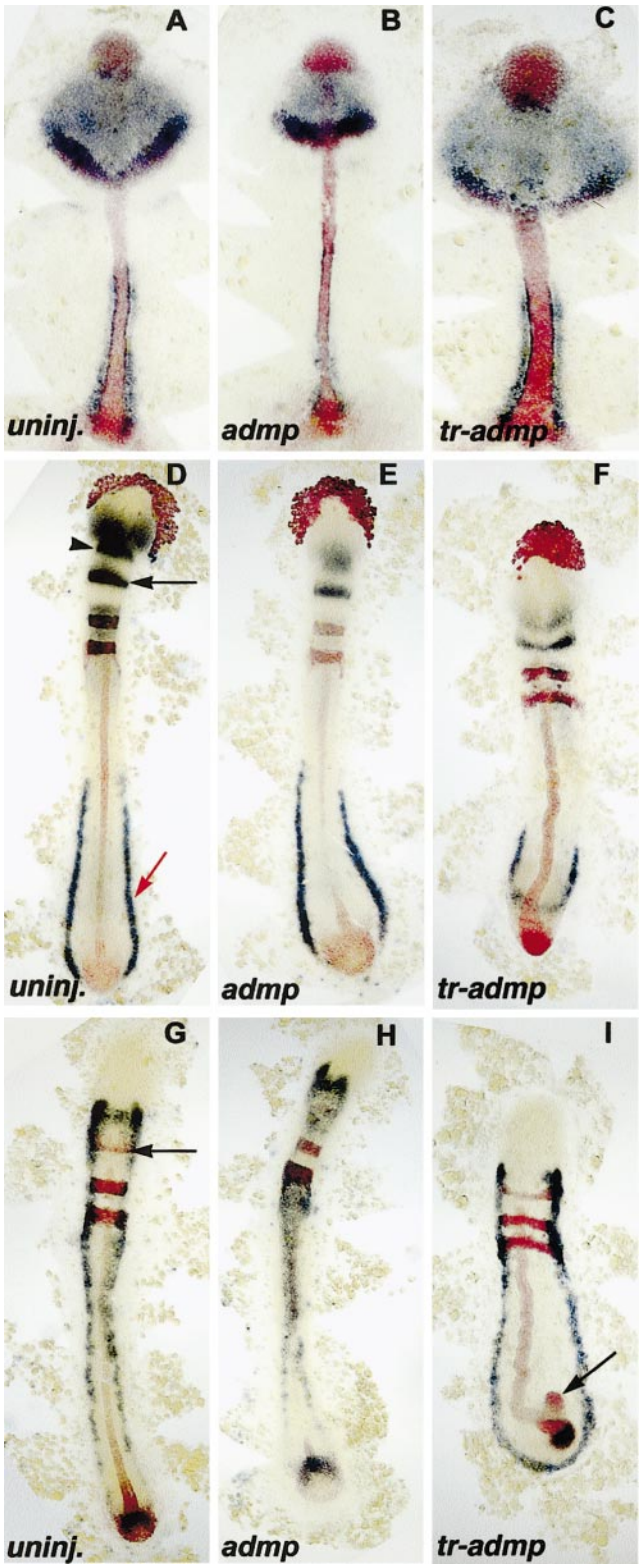

FIG. 4. ADMP and TR-ADMP have opposite effects. *wt* embryos were injected at the one-cell stage with *admp* RNA (600 pg) *or* *tr-admp* RNA (600 pg) and compared to uninjected siblings (*uninj*.). (A–I) Flat mounts of stained embryos, anterior to the top. (A–C) Flat mounts of embryos stained at 95% epiboly with *hgg1*, *ntl*, *her5* probes in red and *otx2*, *myoD* probes in dark blue. (D–F) Flat mounts of embryos stained at the 10-somite stage with *hgg1*, *ntl*, *krox20* probes in red and *pax6*, *her5*, *gata1* probes in dark blue. (D) *her5* (black arrow), *gata1* (red arrow), and the posterior limit of *pax6* expression domain (arrowhead), are indicated. (G–I) Flat mount of embryos stained at the 10-somite stage with *ntl*, *krox20*, *her5* probes in red and *fkd6* probe in dark blue. (G) *her5* domain (black arrow) is indicated. (I) End of the notochord is frequently split in *tr-admp*-injected embryos (arrow).

30)-injected embryos revealed a 40% increase of notochord cells (NTL-positive) upon *tr-admp* injection. This observation allows to distinguish the dorsalized-like phenotype obtained with *tr-admp* or the *admp*-morpholino from the dorsalized phenotype accompanying a loss of *bmp2b* function. Indeed, we did not observe any significant difference in the number of NTL-positive cells between *swirl* homozygous embryos ($n = 5$; 384 cells +/− 35) and wild-type siblings ($n = 5$; 362 cells +/− 35), as previously described (Mullins *et al.*, 1996). We did not observe any significant difference either in the number of NTL-positive cells between *snailhouse* homozygous embryos ($n = 4$; 433 +/− 45) and wild-type siblings ($n = 4$; 396 +/− 22).

Altogether, a comparison between the Mo and *tr-admp* effect revealed that the latter corresponds to a more pronounced enlargement of dorso-axial structures. Moreover, *tr-admp* led to the loss of ventral tail fin and ventral vein not observed upon Mo injection. This difference might be explained by a partial effect of the morpholino or by the interference of *tr-admp* with other *bmps*.

tr-admp Effect Is Reversed by admp and bmp7

To test the dominant-negative properties of TR-ADMP, we explored its ability to counteract the effect of ADMP. Injection of *admp* RNA (600 pg) or *tr-admp* RNA (600 pg) alone resulted in 0 and 6% of embryos with wild-type morphology, respectively. Coinjection of *admp* and *tr-admp* RNAs resulted in 20% of embryos with wild-type morphology (Table 1). Thus, the two forms were able to antagonize each other. However, although *tr-admp* effect was in part reversed by coinjection with *admp* RNA in a dose-dependent manner (data not shown), *tr-admp* was dominant over *admp* as embryos with dorsalized features (loss of ventral tail fin and ventral vein) were always observed in coinjection experiments. This observation suggests an interference of *tr-admp* with some other pathway.

We investigated the ability of TR-ADMP to antagonize the activity of BMP2b and BMP7, to further discuss its specificity. We tested the effects of a truncated form of *bmp2b* (*tr-bmp2b*) missing 44 amino acids at the C-terminal end. Coinjection experiments showed that *bmp2b* and *tr-bmp2b* RNA were able to counteract each

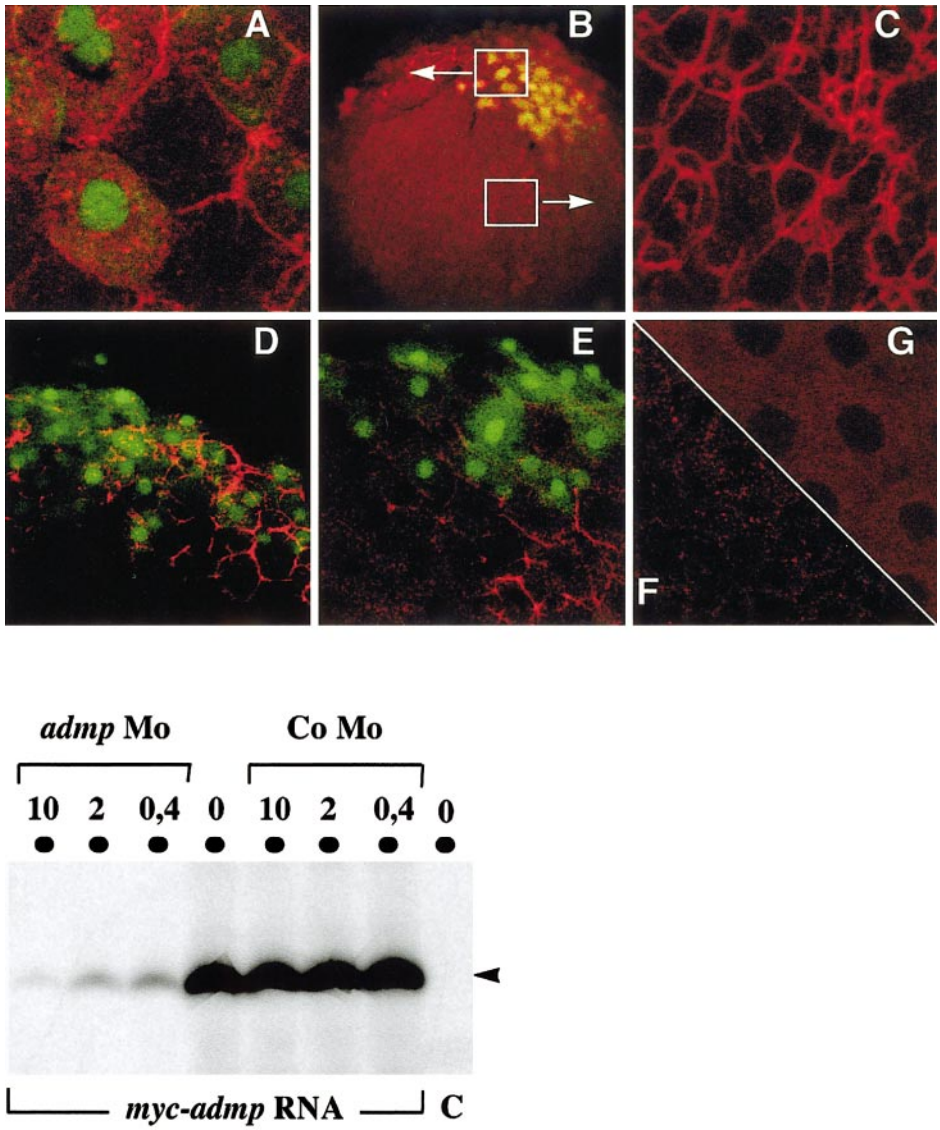

FIG. 5. Detection of the MYC-ADMP protein. (Top panel) *myc-admp* RNA and *nls-gfp* RNA (50 pg) were injected at the 16-cell stage into 1 marginal blatomere, and MYC-ADMP expression was revealed by immunocytochemistry at the sphere stage. NLS-GFP was used as a lineage tracer to identify the progeny of the injected cell. Embryos where observed with a confocal microscope. (A–C) *myc-admp* RNA (200 pg) (B)-injected embryo (10× objective); white boxes indicate a GFP-positive region and a GFP-negative region showed at a higher magnification in (A) and (C), respectively. (A, C, G) 63× objective. (A) Injected embryo, GFP-positive domain. (C) Injected embryo, GFP-negative domain. (G) Uninjected embryo. (D–F) 40× objective. (D–E) *myc-admp* (50 pg) and *nls-gfp* RNA (50 pg) (E) *admp*-morpholino (500μM) was injected at the one-cell stage prior to *myc-admp* and *nls-gfp* RNA injection at the 16-cell stage. (F) Uninjected embryo. (Bottom panel) *myc-admp* RNA (1μg) or no RNA (C) was translated *in vitro* in the absence (0) or in the presence of *admp*-morpholino (10, 2, or 0.4 μg in a reaction volume of 25 μl). The synthesis of MYC-ADMP protein (45 kDa, arrowhead) was inhibited by the *admp*-morpholino (*admp*-Mo) in a dose-dependent manner, and was not affected by the presence of a control morpholino (Co-Mo).

other, giving rise to 54% of wild-type-looking embryos, compared to 25% obtained upon *bmp2b* RNA injection, and 19% upon *tr-bmp2b* RNA injection. On the contrary, coinjection of *bmp2b* and *tr-admp* RNA did not allow the recovery of more wild-type-looking embryos than the separate injections, but produced 45% of phenotypes never observed upon injection of either *bmp2b* or *tr-admp* RNA. These embryos showed both axialized and ventralized features (Fig. 7D). They displayed the entire range of anterior defects observed in *bmp2b*-injected embryos, but showed less notochord defects and were devoid of ventral vein and/or ventral tail fin. Such a phenotype might be explained

by the interference of BMP2b and TR-ADMP with distinct pathways both acting on the dorso-ventral patterning. Thus, TR-ADMP appears to interact with ADMP and not with BMP2b.

The coinjection of *tr-admp* and *bmp7* RNA revealed several striking features. The phenotypic effect of *bmp7* overexpression clearly differed from that of *bmp2b* (Fig. 7). *bmp7* RNA (40 or 160 pg) was injected at the one-cell stage. Living embryos observed after 1 day of development displayed a variable loss of dorso-anterior structures, falling into five classes (Fig. 7, and Table 1). Type I had reduced eyes. Type II had very reduced eyes or no eyes, a shorter body axis, and displayed a variable reduction of ventral tail fin. Type III had no head, a short body axis, no yolk-tube extension, and variable notochord defects. Type IV exhibited a short and thick body axis lying on top of an elongated yolk cell. They had no recognizable head structures but frequently had pieces of notochord and were able to move (Fig. 7H). Type V embryos died during somitogenesis due to a constriction of the yolk cell. *bmp7*-injected embryos were stained with *gata1*, *ntl*, *hgg1*, *pax6*, and *her5* probes at the 15-somite stage (Figs. 7I and 7K). Type II embryos showed a prominent tail bud and no notochord defect, suggesting a dorsalized rather than a ventralized phenotype. In addition, the *gata1* expression domain was not obviously expanded. Antero-posterior patterning of the head appeared unaffected but head structures were reduced (Fig. 7K). Type IV embryos showed a notochord brightly stained with *ntl* and a prospective hatching gland domain stained with *hgg1*. *pax6* and *her5* expression domains were lost. Moreover, the hatching gland domain contacted the notochord consistent with a loss of head structures (Fig. 7I). The *gata1* expression domain was expanded and spread along the A-P axis. Altogether, *bmp7* had a strong head suppressor activity, but did not promote a typical ventralizing effect.

bmp7 and *tr-admp* were able to antagonize each other in a dose-dependent manner (Table 1). *c*-admp* with a mutated cleavage site had the same properties (data not shown). On the contrary, *admp*-morpholino did not counteract *bmp7* RNA effect and in particular did not prevent the embryos from dying during somitogenesis (data not shown). Although we cannot exclude that *bmp7* and *tr-admp* antagonized each other through distinct pathways, these observations strongly suggest that TR-ADMP and BMP7 were able to form heterodimers. Thus, TR-ADMP would interact with ADMP as well as BMP7 and not with BMP2b. Consequently, the *tr-admp* overexpression phenotype probably resulted from TR-ADMP interaction with both BMP7 and ADMP. A comparison between Mo and *tr-admp* effect suggested that TR-ADMP interaction with ADMP was responsible for the increase in notochord cells. As TR-ADMP is expected to bind the ADMP precursor and impair ADMP posttranslational maturation, it should only be active when synthesized in cells expressing *admp*. *tr-admp* RNA injection was performed at the 16-cell stage and the addition of dextran-rhodamine as a lineage tracer allowed the later sorting of embryos according to the position of the injection relative to the dorsal side (Peyrieras *et al.*, 1996). An enlargement of the notochord at the end of gastrulation was observed only in embryos injected dorsally (data not shown). But the loss of ventral tail fin and ventral vein was mainly observed in embryos injected ventrally. These results suggest that enlargement of the notochord resulted from an interaction between TR-ADMP and ADMP rather than with a ventrally expressed BMP. On the contrary, the posterior phenotype (lost of ventral tail fin and ventral vein) was likely to result from an interaction between TR-ADMP and a ventrally expressed BMP such as BMP7.

Altogether, these experiments demonstrate that *admp*, *bmp2b*, and *bmp7* RNAs have distinct effects on dorso-ventral patterning that cannot be described with the same phenotypic classes. TR-ADMP properties are best explained by an interaction with both ADMP and BMP7, suggesting that ADMP and BMP7 form heterodimers. Although eliciting distinct responses, ADMP and the ventralizing BMPs might cooperate in establishing a proper dorso-ventral regionalization.

admp and the Ventralizing bmps Cooperate in the Establishment of Dorso-Ventral Regionalization

Such a cooperation might be tested by coinjection of *admp* and *bmp* RNA. As shown in Table 1, *admp* (100 pg) enhances the ventralizing activity of *bmp2b* (10 or 80 pg). The phenotypes observed after 1 day of development were assigned to the V1–V4 phenotypic classes. Coinjection of *admp* and *bmp7* RNA had a strong ventralizing effect that the separate injections did not have. Moreover, *bmp7* RNA (160 pg) injection alone gave rise to 50% dead embryos after 1 day of development that were strongly ventralized but rescued from dying by coinjection with *admp* RNA (100 pg). The phenotypes observed after 1 day of development fell into the V1–V4 categories typical for *bmp2b* RNA injection. They could be correlated with *in situ* hybridization patterns observed at the 15-somite stage (Figs. 7M). Most of the embryos displayed very reduced anterior structures, severe notochord defects, and showed an expansion of the *gata1* expression domain.

If a cooperation between *admp* and *bmps* occurs, *admp* overexpression in the dorsalized mutant *snailhouse* (*snh*), a mutant allele of *bmp7*, and *tr-admp* or *admp*-morpholino overexpression in the ventralized mutant *chordino* (*din*), a mutant allele of *chordin*, should interfere with the mutant phenotypes (Dick *et al.*, 2000; Schmid *et al.*, 2000; Schulte-Merker *et al.*, 1997; Fisher *et al.*, 1997; Hammerschmidt *et al.*, 1996a). Conversely, *snh* and *din* phenotypes should be enhanced by Mo or *tr-admp* and *admp* overexpression, respectively.

admp RNA was injected at the one-cell stage into the progeny of *snailhouse* heterozygous parents (Fig. 8). The phenotypes were observed either on live embryos after 1 day of development or at the five- to seven-somite stage on fixed embryos subjected to *in situ* hybridization. At 30 hpf,

TABLE 3

admp, tr-admp RNA or Mo Injection in *snailhouse* or *chordino* Mutants

Cross	*admp* mRNA[a]	*n*	% WT	% Class 1	% Class 2	% Class 3	% Class 4	% C1	% C2	% C3	% C4	% Dead
snh −/+ × −/+	0	80	75				0	0	0	0	25	
snh −/+ × −/+ 30 h	600	88		45[b]		21[c]	0		13[d]		11[e]	10
snh −/+ × −/+ 5–7 somites	600	39	38			51[c]				11[f]	0	

cross	*tr-admp*[g]	*n*	% WT	% *din* phenotype	% DV[h]	% A1	% A2	% A3	% A4
din −/− × −/+ 30 h	0	24	50	50					
din −/− × −/+ 30 h	600	176	34	0	18	20	16	2	10

[a] *admp* RNA was injected at the one-cell stage into the progeny of *snailhouse* heterozygotes, and phenotypes were observed after 30 h of development, or at the five- to seven-somite stage.

[b] % WT + class 1.

[c] % class 2 + class 3.

[d] % C1 + C2.

[e] % C3 + C4.

[f] Note that at the five- to seven-somite stage, we only recognized 11% of C2 or C3 dorsalized phenotypes. Given the percentage of dorsalized phenotypes (24%) identified after 30 h of development, we interpret that the C1 phenotypes were scored as wt at the earlier stage.

[g] *tr-admp* RNA was injected at the one-cell stage into the progeny of a din −/− × din −/+ cross.

[h] Embryos having a ventralized phenotype also exhibited dorsalized features (DV), see Fig. 9B.

dorsalized phenotypes were characterized according to previous descriptions (Mullins *et al.*, 1996). The uninjected siblings displayed 25% of C4 phenotype (Mullins *et al.*, 1996; Nguyen *et al.*, 1998). *admp* injection led to the recovery of C1 or C2 phenotypes at the expense of the C4 ones (Table 3). Thus, *admp* RNA was able to partially rescue the *snailhouse* phenotype. These embryos, although still dorsalized, had a smaller head typical of the *admp* phenotype, and not observed in the *snailhouse* mutants, showing that *admp* does not mimic *bmp7* function. A partial rescue of the *snailhouse* phenotype was confirmed by the observation of the five- to seven-somite-stage embryos (Fig. 8, and Table 3). At this stage, the *snailhouse* C4 phenotype is characterized by the radialized expression of *myoD* and *krox 20* (Fig. 8). We did not observe any C4 phenotype in the injected population, but identified 11% of embryos with a protruding tail bud and enlarged somites, corresponding to a C3 or C2 dorsalized phenotype (Table 3). Altogether, these results indicate a partial rescue of the C4 phenotype to a C3, C2, or even C1 phenotype and suggest that *admp* RNA is able to counteract the expansion of dorsal structures in *snailhouse* mutants. Conversely, *tr-admp* RNA (600 pg) or *admp*-morpholino (250 μM) injected at the one-cell stage into the progeny of *snh* heterozygous parents enhanced the dorsalized phenotype of homozygous embryos (Figs. 8G–8I, and data not shown). At the six-somite stage, *tr-admp* RNA- or *admp*-morpholino (not shown)-injected *snh* homozygous embryos showed a radialized expression of *her5* and *krox 20*. *fkd6* expression was confined to the tip of the tail. These features indicated a strongly dorsalized phenotype. The injected *snh* homozygous embryos died during somitogenesis, consistent with a C5 phenotype.

tr-admp RNA (600 pg) or *admp*-morpholino (250 μM) was injected at the one-cell stage into the progeny of a $din^{-/-} \times din^{-/+}$ cross. Living embryos were observed after 1 day of development or fixed and processed for *in situ* hybridization at the 10-somite stage (Fig. 9). The uninjected siblings displayed 50% of ventralized phenotype. As shown in Table 3, *tr-admp* RNA injection was able to rescue or dorsoaxialize the *din* mutants. *admp*-morpholino injection also improved the *din* phenotype albeit less efficiently than *tr-admp* RNA and did not give rise to a loss of ventral tail fin (Fig. 9D). A partial rescue of the *chordino* mutant phenotype was confirmed by the observation of the 10-somite-stage embryos (Figs. 9H–9I). Conversely, *admp* RNA injection enhanced the ventralized phenotype of *din* homozygous mutants (Fig. 9C). *In situ* hybridization performed at the 10-somite stage showed that injected *din* homozygous embryos had more severe notochord defects (Figs. 9F and 9G).

These observations confirm that a proper dorso-ventral regionalization can be achieved through the balance of ADMP and BMP activities. Moreover, the remarkable synergy of ADMP and BMP7 in coinjection experiments is another argument in favor of the hypothesis that they form heterodimers.

Formation of Dorso-Anterior Structures Is Favored by Low Levels of bmp and admp Expression

We hypothesize that *admp* expression is regulated as an organizer-specific gene and counteracts the formation and

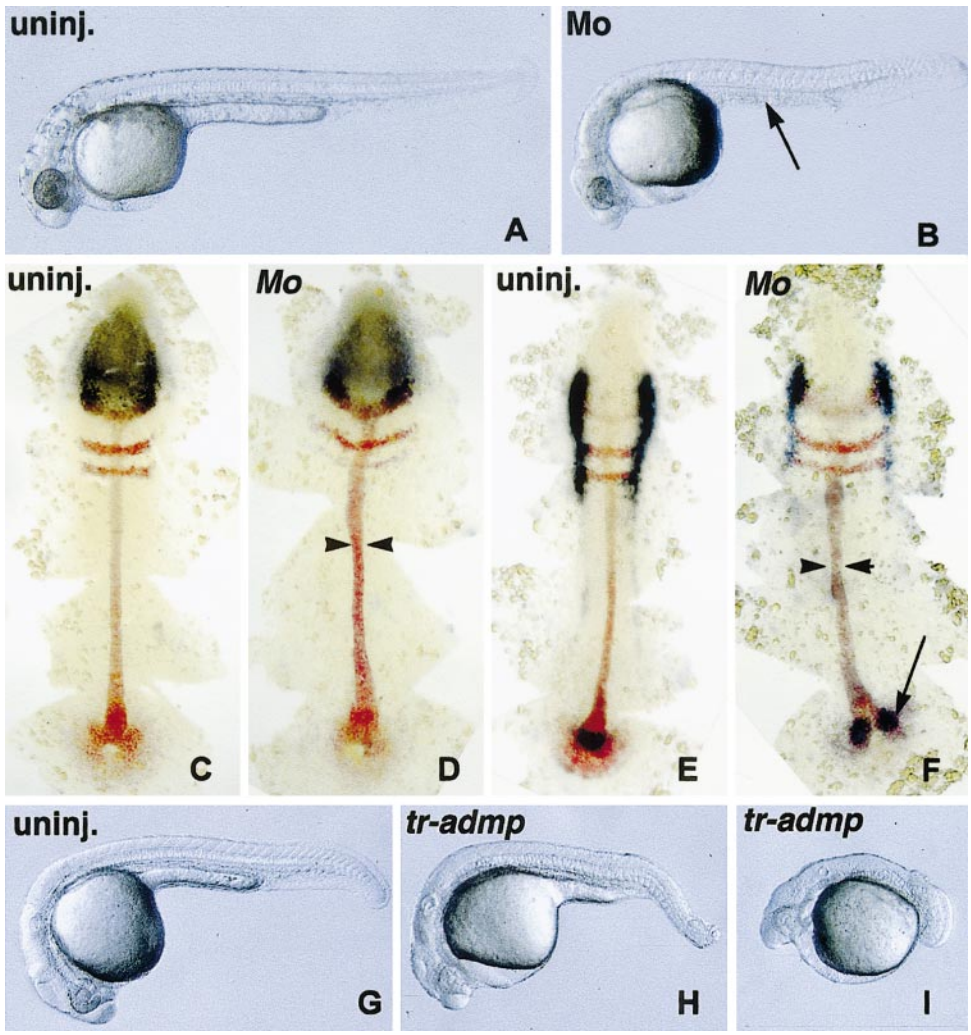

FIG. 6. *admp*-morpholino and *tr-admp* RNA promote the expansion of dorso-axial structures. *wt* embryos were injected at the one-cell stage with *admp*-morpholino (Mo) (250 μM) or *tr-admp* RNA (600 pg) and compared to uninjected siblings (uninj.). Embryos injected with a control morpholino were unaffected (not shown) and similar to uninjected siblings. (A, B, G–I) Live embryos at 1 day of development. (A) Uninjected embryo. (B) Mo-injected embryos lack the yolk-tube extension (arrow). (C, D) Flat mounts of embryos stained at the three-somite stage with *her5*, *krox20*, *ntl* probes in red and *otx2* probe in dark blue. (E, F) Flat mounts of embryos stained at the three-somite stage with *her5*, *krox20*, *ntl* probes in red and *fkd6* probe in dark blue. (D, F) Mo-injected embryos have an enlarged notochord (arrowheads). (F) End of the notochord is split in Mo-injected embryos (arrow). (G) Uninjected embryo. (H) *tr-admp*-injected embryo, A2 phenotype. (I) *tr-admp*-injected embryo, A3 phenotype. Note the loss of ventral tail fin and vein in *tr-admp*-injected embryos that is not observed upon Mo injection.

expansion of anterior and axial fates, behaving as an antagonist of organizer function. We used a system of secondary axis induction to investigate these points.

We previously showed that injection at the 16-cell stage into one marginal blastomere of RNA encoding TAR*, a constitutively active form of the type I receptor kinase TARAM-A, induced a secondary shield giving rise to a complete embryonic axis in 100% of the embryos injected in a ventrally fated blastomere (Peyrieras *et al.*, 1996). We therefore examined *admp* expression in *tar** (2 pg)-injected embryos, and found that it was induced at the shield stage, in a limited area, at the margin of the blastoderm (Fig. 10D). *admp* expression was also induced at the margin of the blastoderm after injection of RNA encoding the transcription factor *boz/dharma* (2 pg) (Fig. 10B), known to elicit a complete axis induction (Fekany *et al.*, 1999; Koos and Ho, 1998; Yamanaka *et al.*, 1998). These results suggest that *admp* expression is regulated by both the NODAL/ACTIVIN and β-CATENIN pathways. In addition, *in situ* hybridization with an *admp* probe was performed on *mzoep*

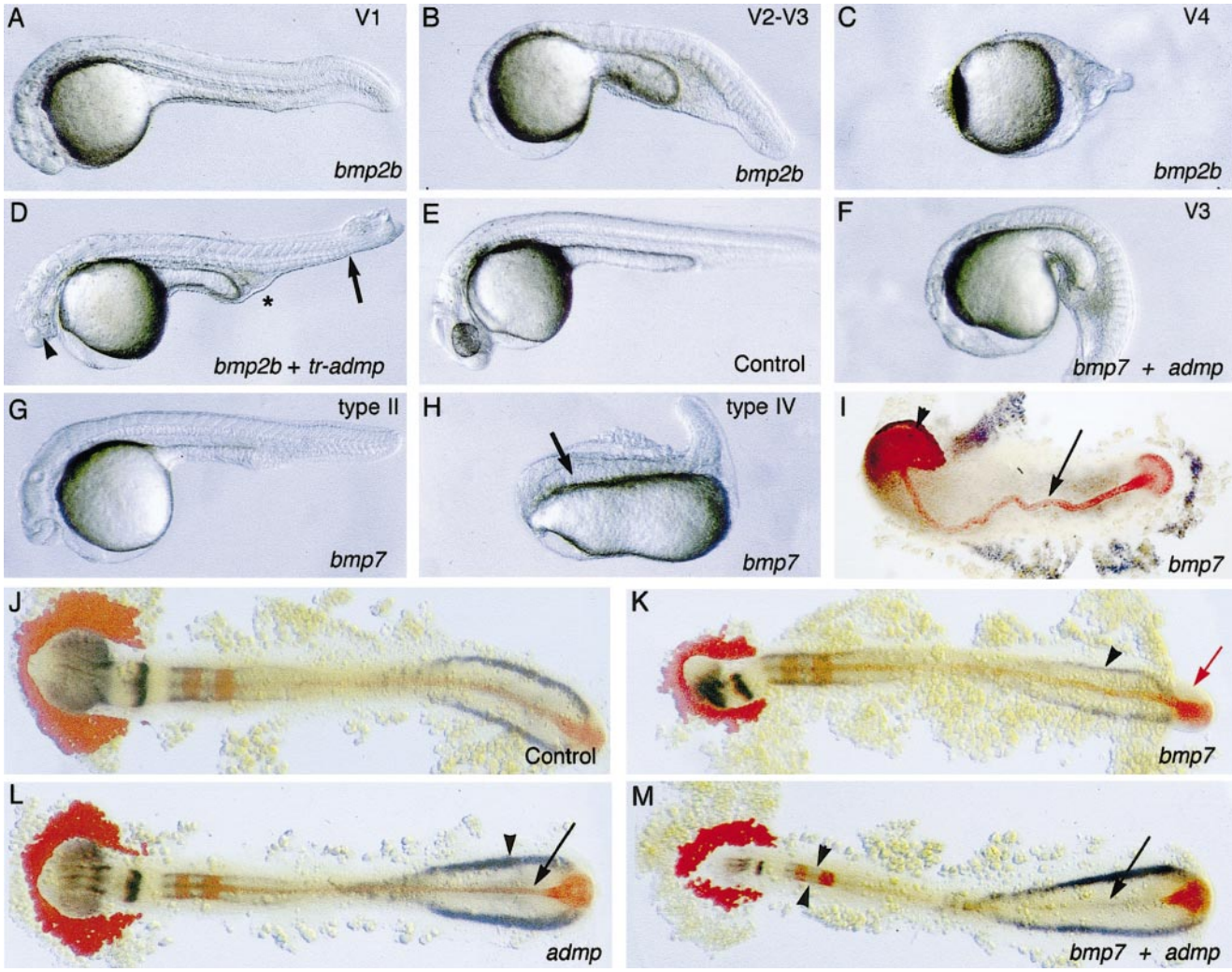

FIG. 7. *admp*, *bmp2b*, and *bmp7* have distinct effects. *wt* embryos were injected at the one-cell stage with *bmp2b*, *bmp7*, *admp*, or *tr-admp* RNA either alone or in combination (*bmp2b* + *tr-admp* or *bmp7* + *admp*) compared to uninjected siblings (control). (A–H) Live embryos at 1 day of development. (I–M) Flat mounts of embryos stained at the 15-somite stage with *pax6*, *her5*, and *gata1* in dark blue; *hgg1*, *krox20*, and *ntl* in red; anterior to the left. (A–C) *bmp2b* RNA-injected embryos with V1, strong V2 (designated V2–V3), or V4 phenotype. (D) Embryos coinjected with *bmp2b* and *tr-admp* display both dorsalized (loss of the ventral tail fin and ventral vein indicated by an arrow) and ventralized features (reduced head indicated by an arrow head, excess of blood cells marked "*"). (F) Embryos coinjected with *bmp7* and *admp* display a typical ventralized phenotype. (G, H) *bmp7* RNA-injected embryos with type II and type IV phenotype. (H) The notochord is indicated (arrow). (I, K) *bmp7*-injected embryos. (I) The notochord (arrow) and the hatching gland (arrowhead) are indicated. (K) The prominent tail bud (red arrow) and unaffected *gata1* expression domain (arrowhead) are indicated. (L) *admp*-injected embryo. *ntl* staining is reduced (arrow) and *gata1* is expanded (arrowhead). Compare with (J). (M) *bmp7* and *tr-admp* RNA coinjected embryo. The posterior notochord is lost (arrow) and the neural plate reduced (arrowheads). Numbers and doses corresponding to this experiment are reported in Table 1.

embryos, devoid of maternal and zygotic *oep* function required for nodal signalling, and *boz* homozygous mutants (Fekany *et al.*, 1999; Gritsman *et al.*, 1999). *admp* RNA expression was unaffected at the sphere stage, but was reduced in both mutants at the onset of gastrulation (Fig. 10E, and data not shown). These observations suggest that *boz* and *oep* pathways are involved in the maintenance of *admp* expression in the organizer region. In this respect, *admp* behaves as an organizer-specific gene. Moreover, we found that coinjection with *admp* RNA abolished the ability of *tar** RNA to induce secondary axial structures (data not shown). Thus, in this experimental system, ADMP behaves as a potent antagonist of organizer function.

Conversely, interference with *admp* function should fa-

vor the formation of an embryonic axis. This was studied in a system of secondary axis induction upon injection at the 16-cell stage, into one marginal blastomere of mouse Δ-*alk3* RNA, that encodes a truncated form of the BMP type I receptor Δ-ALK3 with dominant-negative activity. Consistent with previous results obtained in *Xenopus* (Dosch and Niehrs, 2000; Glinka *et al.*, 1997), Δ-*alk3* RNA injection led to partial secondary axis induction (11/140). The secondary embryonic axis lacked anterior structures and midline structures (Figs. 11A and 11B) and we hypothesize that ADMP activity is responsible for these defects.

We observed that *admp* was induced in response to the injection of Δ-*alk3* RNA (150 pg) and even more efficiently by Δ-*alk6* RNA (25 pg), encoding a dominant-negative form of another BMP type I receptor (Fig. 10C) (Nikaido *et al.*, 1999). These results show that a negative interference with the BMP pathway at the blastoderm margin leads to the expression of *admp*. ADMP protein could counteract the formation of axial structures in the induced secondary embryonic axis. In that case, *admp*-morpholino RNA injection should favor the formation of dorso-anterior structures in the secondary axis induction elicited in response to the injection of mouse Δ-*alk3* RNA. This is what we observed. In order to prevent ADMP secretion both from the endogenous expression domain and from the induced one, the *admp*-morpholino was injected at the one-cell stage followed by the injection of mouse Δ-*alk3* RNA into one marginal blastomere at the 16-cell stage. This led to secondary axis induction (11/128). *In situ* hybridization performed after 1 day of development with *pax6* and *her5* probes revealed the presence of forebrain tissues upon Mo injection that were not found with mouse Δ-*alk3* RNA injection alone (Figs. 11B and 11C).

These results indicate that a negative interference with ADMP secretion throughout the embryo favors the formation of anterior head structures in the secondary axis elicited in response to a local inhibition of the BMP pathway at the margin of the blastoderm.

DISCUSSION

admp Structure, Expression Domain, and Function Are Largely Conserved

admp was previously described in *Xenopus* and chick. We report here its characterization in zebrafish. *admp* structure and expression domain appear to be largely conserved. Our study emphasizes the role of ADMP in the inhibition of anterior and axial structures, also described as an inhibition of organizer activity, and the link between this aspect of antero-posterior patterning and the regulation of dorso-ventral fates.

In zebrafish, *admp* is zygotically expressed on the dorsal side of the blastula. At the onset of gastrulation, expression is restricted to the organizer region. This is comparable to its expression in the dorsal blastopore lip in *Xenopus* and in the node epiblast in the chick (Joubin and Stern, 1999; Moos *et al.*, 1995). Expression in the zebrafish tail bud during somitogenesis fits with its posterior expression in *Xenopus* embryos at stage 22 (Moos *et al.*, 1995). Thus, *admp* might play a role in the tail organizer in both organisms. It might be different in the chick, where its expression is rapidly down-regulated in the node as the head process starts to form (Joubin and Stern, 1999).

The phenotypes observed in *admp* overexpression experiments were characterized by the loss of dorso-axial derivatives affecting the whole embryonic axis. We emphasized *admp* effect on the formation of the notochord that is a midline structure. *admp* phenotype showed fused somites and a shortened tail as observed in *ntl* mutants, consistent with the loss of *ntl* expression (Schulte-Merker *et al.*, 1994). However, observed phenotypes did not correspond to a mere loss of midline structures. We did not find cyclopic embryos that would indicate the loss of prechordal plate and ventral brain structures. Neuroectoderm was also affected as we observed a variable reduction of the head and anterior structures were eventually lost in the strongest phenotypes. Altogether, *admp* overexpression effects in zebrafish are similar to those described in *Xenopus* (Moos *et al.*, 1995).

ADMP- and BMP-Mediated Pathways Have Distinct Effects

The phenotypes observed upon *admp* RNA injection were reminiscent of those observed in *bmp* overexpression experiments. Overexpression of *admp* RNA caused a reduction of the expression domain of dorsal markers during gastrulation in both mesodermal and neuroectodermal germ layers (*floating head* and *chordino* analyzed at the shield stage and, *forkhead 3* at 75% epiboly; data not shown). In this respect, overexpression of *admp* and *bmp2b* RNA have similar effects. But analysis at later stages allowed their action to be distinguished. In particular, whereas overexpression of *bmp2b* RNA led to the reduction of anterior structures, leaving the notochord unaffected (V1 phenotype) (Kishimoto *et al.*, 1997; Nguyen *et al.*, 1998), overexpression of *admp* disrupted notochord development without dramatically affecting anterior structures (class 1 or class 2 phenotypes). The difference between *bmp7* and *admp* phenotypic effects was even more striking. Most of the *bmp7*-injected embryos had no head but retained part of the notochord. They also frequently had a reduced ventral tail fin, rather indicating a dorsalized phenotype. We conclude from these observations that ADMP, BMP2b, and BMP7 have a distinct effect. Hence, ADMP and BMP7 cannot be described as typical ventralizing agents.

admp loss-of-function studies provided other arguments in favor of a distinct action. The specificity of *tr-admp* was investigated by coinjection experiments with either *admp*, *bmp2b*, or *bmp7* RNA. TR-ADMP was able to counteract ADMP and BMP7 but not BMP2b activity. This antagonistic effect is better explained by the formation of TR-ADMP/BMP7 heterodimers. This idea is consistent with the observation that the *admp*-morpholino did not counteract *bmp7*

effect. Thus, TR-ADMP is likely to act as dominant-negative form of both ADMP and BMP7.

The ventral injection of *tr-bmp2b* RNA induced a partial secondary embryonic axis and this was never observed upon *tr-admp* RNA injection (data not shown). In addition, *tr-admp* RNA overexpression led to the expansion of axial fates, as we observed an increase of the presumptive notochord cells (*ntl*-positive). As shown previously, this was not observed in *swirl* mutants, where the enlargement of the notochord was rather thought to be the consequence of convergence extension defects (Mullins *et al.*, 1996). This was not observed in *snh* mutants either, indicating that a loss of *bmp7* was not sufficient to produce this effect. The *admp* morpholino allowed us to confirm that a loss of *admp* function caused an increase of the presumptive notochord cells. This effect might be explained either by a role of *admp* in cell proliferation or by its involvement in the recruitment of cells into the notochord.

We conclude from these observations that *admp* overexpression leads to a loss of axial structures along the antero-posterior axis rather than to a ventralization of the embryos. Our results suggest that ADMP primarily has an inhibitory activity affecting anterior and axial derivatives, the tail and trunk ones being possibly more sensitive to its effect than more anterior structures. Such a role fits with the presence of *admp* RNA in the organizer at the onset of gastrulation, in the anterior neuroectoderm and the endomesodermal layer along the antero-posterior axis during gastrulation and at the tip of the growing notochord during somitogenesis. This interpretation differs from the recent suggestion that *Xenopus* ADMP promotes a trunk organizer activity and inhibits the head organizer (Dosch and Niehrs, 2000).

admp, bmp7, and bmp2b Cooperate in Establishing Dorso-Ventral Fates

A cooperation between ADMP and other so-called ventralizing BMPs might occur through indirect mechanisms. By eliciting a reduction of the expression domain of *chordin*, *admp* RNA should favor the expansion of ventral fates. Consistently, we showed that the expansion of axial fates promoted by the *admp*-morpholino injection was able to compensate the ventralization induced by *chordino* loss-of-function. This might be explained by an increase in some other BMP antagonist.

On the other hand, *admp* partially rescued the radialized expression of several markers (*pax2.1*, *krox20*, *myoD*) observed during somitogenesis in *snailhouse* mutants. *admp* injection also slightly improved the phenotype of homozygous *swirl* embryos, affected in *bmp2b* function (Kishimoto *et al.*, 1997; Nguyen *et al.*, 1998), but did not prevent them from dying during somitogenesis (not shown). Although ADMP could not substitute for BMP7/SNAILHOUSE or BMP2b/SWIRL, *admp* RNA overexpression was able to counteract the expansion of dorsal fates observed in the dorsalized mutants.

A cooperation between ADMP and other ventralizing BMPs (BMP2b, BMP4, BMP7) might occur through the formation of heterodimers in the domains where they are coexpressed. BMP2b and BMP4 were hypothesized to form heterodimers with BMP7 (Schmid *et al.*, 2000). XBMP7 was shown to form heterodimers with mNODAL (Yeo and Whitman, 2001). Our experiments indicate that ADMP and BMP7 might form heterodimers as well. Biochemical studies are currently performed to test this hypothesis and further investigate the ability of ADMP to interact with other BMPs or even with NODAL/ACTVIN molecules, as well as to explore the binding affinity of homodimers and heterodimers for various receptors. Nevertheless, we hypothesize that ADMP/BMP7 heterodimers with a strong ventralizing or head-suppressor activity are secreted by the prechordal plate cells during gastrulation.

We conclude that ADMP- and BMP-mediated pathways cooperate in establishing dorso-ventral fates, through their respective abilities to restrict the expansion of anterior and

FIG. 8. Overexpression of *admp* or *tr-admp* RNA and in *snailhouse*. *admp* RNA (600 pg) or *tr-admp* RNA (600 pg) was injected at the one-cell stage into the progeny of *snailhouse* heterozygous fish. (A–C) Phenotypes were observed live after 1 day of development or (D–I) after *in situ* hybridization. (D–F) *pax 2.1* and *myo D* in dark blue, *hgg1* and *krox 20* in red at the five- to seven-somite stage. (G–I) *her5* and *fkd6* in dark blue, *hgg1*, *krox 20*, and *ntl* in red at the six-somite stage. (A) Uninjected, −/+ or +/+ embryo. (B) Uninjected, *snailhouse* C4 phenotype. (C) *admp*-injected *snailhouse* mutant, C2 phenotype. (B, C) The eye is reduced in (C), compare with (B) (arrowhead). (D, G) Uninjected, −/+ *or* +/+ embryo. (E) Uninjected, *snailhouse* C4 phenotype. (F) *admp*-injected homozygous *snailhouse* embryo, C2 phenotype. (H) Uninjected, *snailhouse* C4 phenotype. The neural crest is expanded. (I) tr-*admp*-injected homozygous *snailhouse* embryo, C5 phenotype.

FIG. 9. Overexpression of *admp*, *tr-admp*, or *admp*-morpholino in *din* mutants. *tr-admp* RNA (600 pg), *admp* RNA (600 pg), or *admp*-morpholino (Mo) (250 μM) was injected at the one-cell stage into the progeny of a $din^{-/-} \times din^{-/+}$ cross. (A–D) Phenotypes were observed live after 1 day of development or (E–I) after *in situ* hybridization at the 10-somite stage; *fkd6*, *her5*, and *gata1* in dark blue, *hgg1*, *krox20*, and *ntl* in red. (A) Uninjected embryo, $din^{-/-}$ phenotype. (B) *tr-admp*-injected $din^{-/-}$ embryo, partially rescued. (C) *admp* injected $din^{-/-}$ embryo, enhanced phenotype. (D) Mo-injected $din^{-/-}$ embryo, partially rescued. (A–D) Arrowhead, compare the size of the eye; arrows, ventral tail fin and vein, lost in (B); and amount of blood cells slightly reduced in (B) and (D). (E) Uninjected, −/+ *or* +/+ embryo. (F) Uninjected embryo, $din^{-/-}$ phenotype. *gata1* expression domain is enlarged (arrowhead) (G) *admp* injected $din^{-/-}$ embryo, enhanced phenotype. Note the absence of posterior notochord (arrow) and the enlarged *gata1* expression domain (arrowhead). (H) Mo-injected $din^{-/-}$ embryo, partially rescued. The notochord is enlarged (arrow); compare with (A) and (B). (I) *tr-admp*-injected $din^{-/-}$ embryo, partially rescued. The notochord is enlarged (arrow).

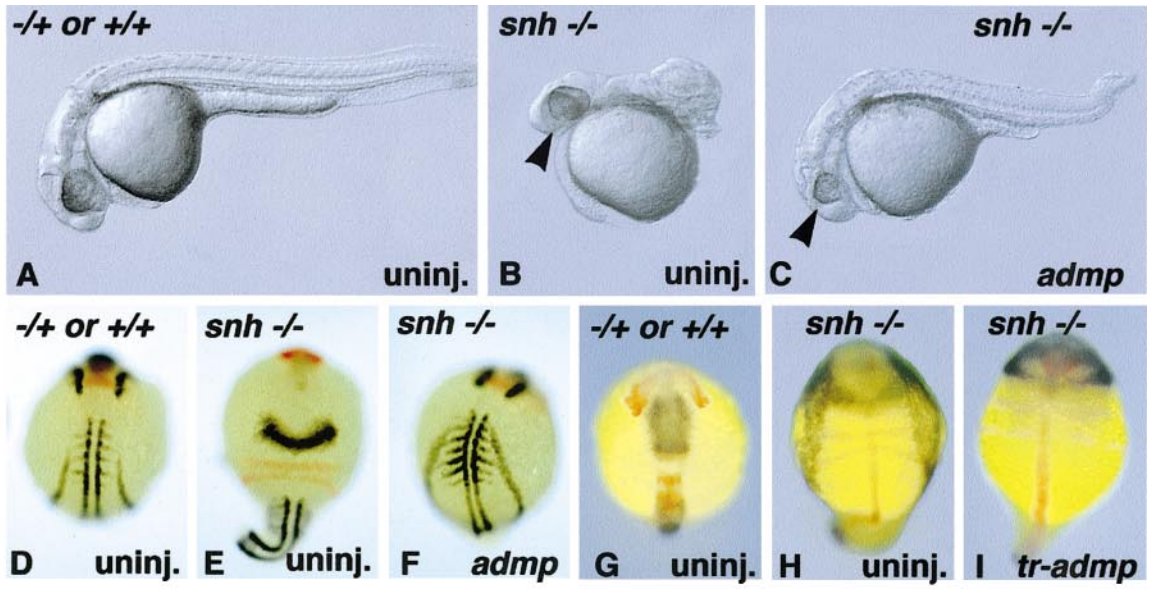

8

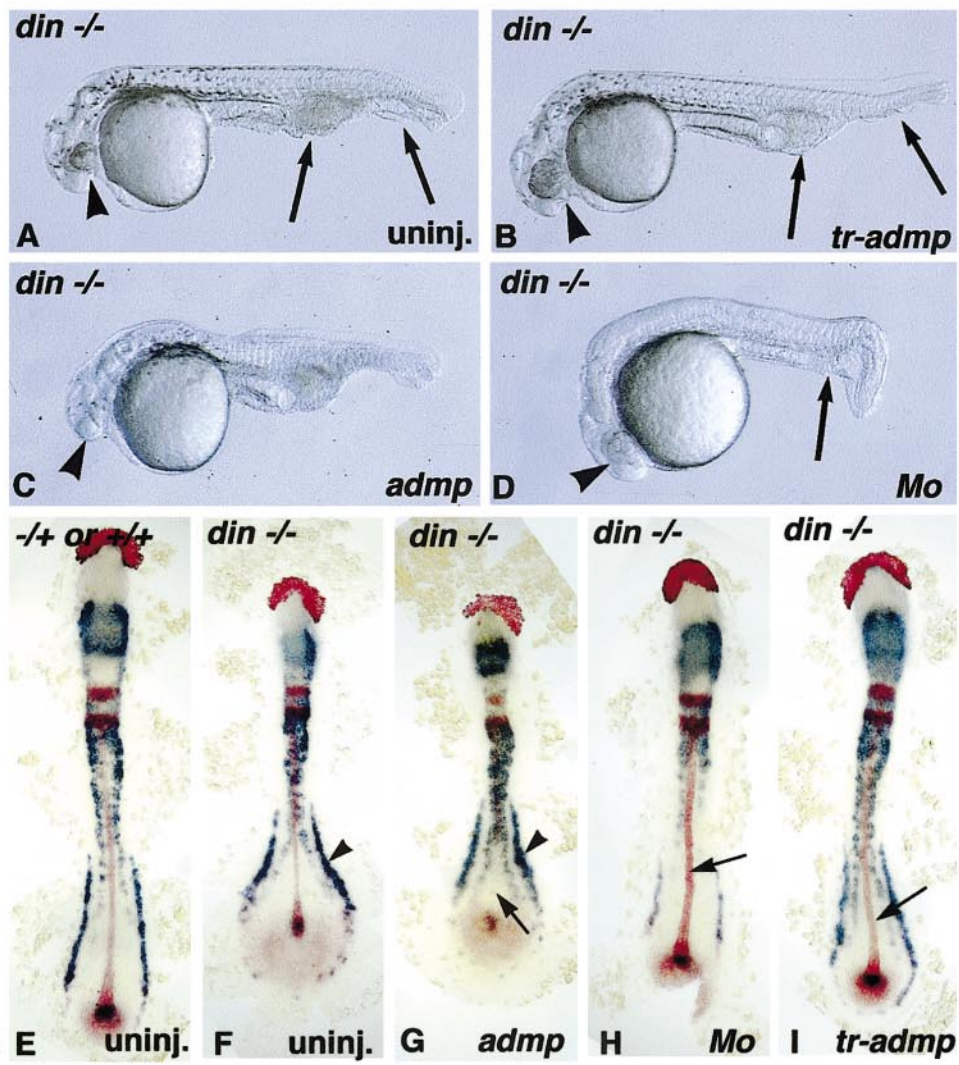

9

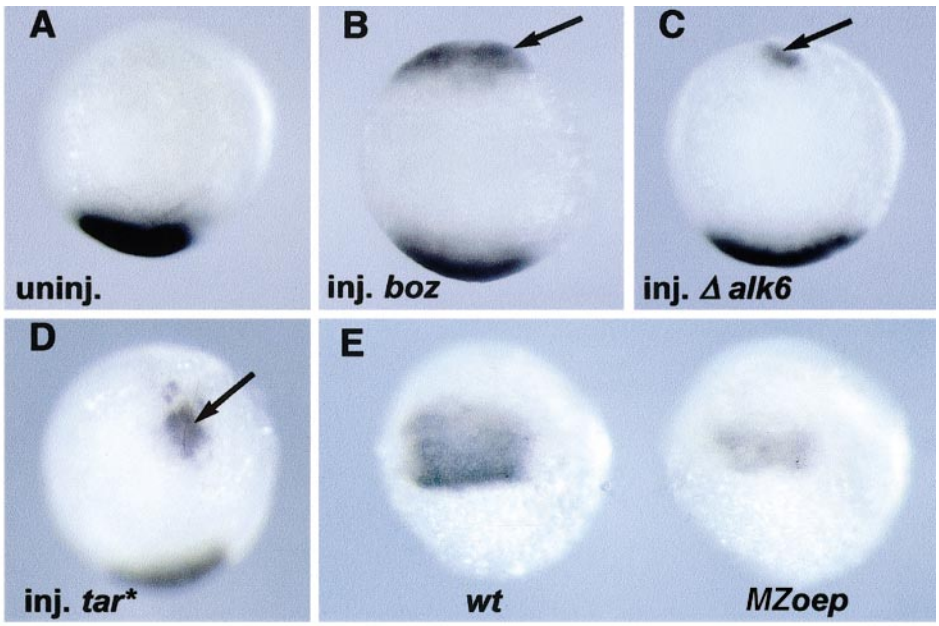

10

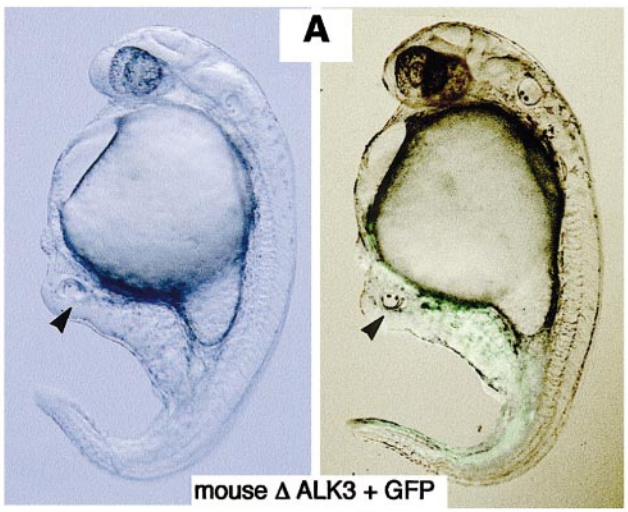

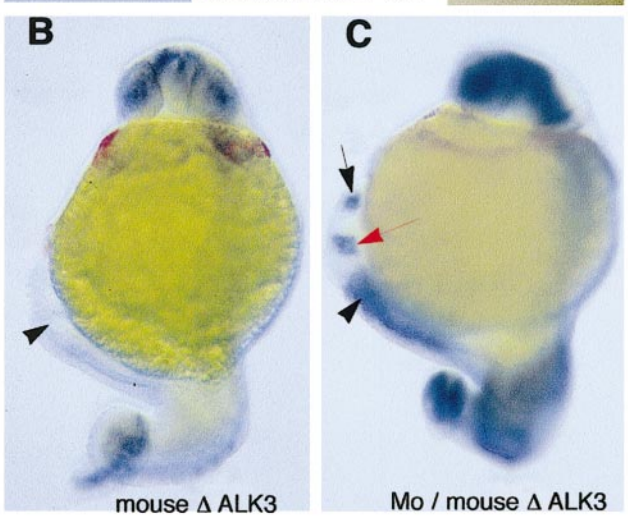

11

axial fates and to promote the expansion of ventral ones as well as through the formation of heterodimers.

ADMP Diffusion in Vivo

We used a tagged form of ADMP to study the subcellular localization of the protein. MYC-ADMP biological activity was similar to that of ADMP. MYC-ADMP was efficiently secreted, and present in the extracellular space far from the secreting cells. This was never observed previously for other tagged TGF-β-like molecules. For example, ACTIVIN diffusion was not detected in a comparable experimental system (Reilly and Melton, 1996). Our observations demonstrate a long-range diffusion of MYC-ADMP, suggesting that ADMP diffuses *in vivo* as well.

ADMP diffusion *in vivo* is supported by the observation of embryos injected ventrally with Δ-*alk3* RNA, and dorsally with *tr-admp* RNA (data not shown), demonstrating that the inhibition of ADMP secretion on the dorsal side of the embryo favors the formation of anterior head structures in the secondary axis induced ventrally.

The Role of ADMP in Patterning the Zebrafish Organizer

Formation of the organizer on the dorsal side of the embryo is favored by an interference with the BMP pathway. *boz*, acting as a *bmp* repressor, and CHORDIN acting as a BMP antagonist play this role *in vivo* (Gonzalez *et al.*, 2000; Koos and Ho, 1999). This was achieved through Δ-*alk3* RNA injection in our experimental system. The double interference, at the ventral margin of the embryo, with both the *admp* and *bmp* pathways, favors the formation of dorso-anterior structures. Anyway, the formation of anterior head on the ventral side of the embryo was not observed with the coinjection of Δ-*alk3* and *tr-admp* RNA (data not shown). This situation differs from what was described in *Xenopus*, where, in such coinjections, cyclopic heads were induced ventrally (Dosch and Niehrs, 2000).

To induce the formation of forebrain, we had to inhibit ADMP secretion in the whole embryo. This was achieved by using the *admp*-morpholino rather than *tr-admp* RNA, as the latter probably interfered with other pathways. The embryonic axis induced ventrally exhibited forebrain structures. However, its overall morphology indicated defects in convergence extension movements and in the formation of axial mesendoderm. These observations suggest that, although favored by a concomitant inhibition of ADMP and BMP pathways, the formation of dorso-anterior structures requires positive signals expressed on the dorsal side of the embryo and possibly including WNT inhibitors and NODAL molecules.

In conclusion, our results indicate that ADMP participates in a network of positive and negative signals that restrict and maintain the organizer domain. ADMP modulates the organizer activity by regulating the expansion of axial and anterior fates. Through its anti-dorsalizing activity, ADMP also acts on the regulation of dorso-ventral fates and cooperates with BMP signalling. Moreover, ADMP and BMP7 are likely to form heterodimers with a potent ventralizing and head-suppressor activity.

ACKNOWLEDGMENTS

We thank M. Rebagliati and I. Dawid for the gift of the cDNA library, L. Bally-Cuif, A. Fjose, M. Halpern, D. Kimelman, J. Odenthal, N. Ueno, S. Schulte-Merker, B. Thisse, C. Thisse, and E. Weinberg for plasmids and S. Schulte-Merker for the anti-NTL antibody. We are especially grateful to Laure Bally-Cuif, Marnie Halpern, and Philippe Herbomel for critical reading of the manuscript. We are grateful to F. Chelghoum and F. Bouallague for care of the fish. This work was supported by a grant from ARC to F.R.

REFERENCES

Bisgrove, B. W., Essner, J. J., and Yost, H. J. (1999). Regulation of midline development by antagonism of lefty and nodal signaling. *Development* **126,** 3253–3262.

D'Amico, L. A., and Cooper, M. S. (1997). Spatially distinct domains of cell behavior in the zebrafish organizer region. *Biochem. Cell Biol.* **75,** 563–577.

Detrich, H. W., 3rd, Kieran, M. W., Chan, F. Y., Barone, L. M., Yee, K., Rundstadler, J. A., Pratt, S., Ransom, D., and Zon, L. I. (1995).

FIG. 10. *admp* induction at the blastoderm ventral margin. (A–E) *In situ* hybridization with an *admp* probe at the shield stage. (A–D) Embryos were injected at the 16-cell stage into one marginal blastomere *with nls-gfp* RNA as a lineage tracer, sorted according to the position of the injection relative to the dorsal side. Ventrally injected embryos were processed for *in situ* hybridization (animal pole views, ventral to the top). (A) Uninjected embryo. (B) Ventral injection of *boz* RNA (2 pg). (C) Ventral injection of Δ *alk6 RNA* (25 pg). (D) Ventral injection of *tar** RNA (2 pg). Arrows indicate the induced *admp* expression domain. (E) Progeny of an $oep^{-/-} \times oep^{-/+}$ cross. Fifty percent of the embryos (*MZoep*) had a reduced *admp* expression domain compared with wild-type siblings (*wt*).

FIG. 11. *admp* antagonizes organizer formation and maintenance. (A, B) Injection of mouse Δ-*alk3* RNA at the 16-cell stage into one marginal blastomere leads to induction of a partial secondary axis. Arrowheads, otic vesicles. (A) Bright-field and epifluorescence images are shown side by side. The use of NLS-GFP as a lineage tracer reveals the induced axis. (B, C) *In situ* hybridization with *pax6*, *her5*, and *myoD* probes in dark blue, *hgg1* in red. (C) *admp*-morpholino injection at the one-cell stage followed by mouse Δ-*alk3* RNA injection at the 16-cell stage leads to induction of a partial secondary axis with forebrain structures. The forebrain stained with *pax6* (black arrow) and midbrain–hindbrain boundary stained with *her5* (red arrow) are indicated.

Intraembryonic hematopoietic cell migration during vertebrate development. *Proc. Natl. Acad. Sci. USA* **92,** 10713–10717.

Dick, A., Hild, M., Bauer, H., Imai, Y., Maifeld, H., Schier, A. F., Talbot, W. S., Bouwmeester, T., and Hammerschmidt, M. (2000). Essential role of Bmp7 (snailhouse) and its prodomain in dorsoventral patterning of the zebrafish embryo. *Development* **127,** 343–354.

Dosch, R., and Niehrs, C. (2000). Requirement for anti-dorsalizing morphogenetic protein in organizer patterning. *Mech. Dev.* **90,** 195–203.

Fekany, K., Yamanaka, Y., Leung, T., Sirotkin, H. I., Topczewski, J., Gates, M. A., Hibi, M., Renucci, A., Stemple, D., Radbill, A., Schier, A. F., Driever, W., Hirano, T., Talbot, W. S., and Solnica-Krezel, L. (1999). The zebrafish bozozok locus encodes Dharma, a homeodomain protein essential for induction of gastrula organizer and dorsoanterior embryonic structures. *Development* **126,** 1427–1438.

Fisher, S., Amacher, S. L., and Halpern, M. E. (1997). Loss of cerebum function ventralizes the zebrafish embryo. *Development* **124,** 1301–1311.

Funayama, N., Fagotto, F., McCrea, P., and Gumbiner, B. M. (1995). Embryonic axis induction by the armadillo repeat domain of beta-catenin: Evidence for intracellular signaling. *J. Cell Biol.* **128,** 959–968.

Glinka, A., Wu, W., Onichtchouk, D., Blumenstock, C., and Niehrs, C. (1997). Head induction by simultaneous repression of Bmp and Wnt signalling in Xenopus. *Nature* **389,** 517–519.

Gonzalez, E. M., Fekany-Lee, K., Carmany-Rampey, A., Erter, C., Topczewski, J., Wright, C. V., and Solnica-Krezel, L. (2000). Head and trunk in zebrafish arise via coinhibition of BMP signaling by bozozok and chordino [In Process Citation]. *Genes Dev.* **14,** 3087–3092.

Gritsman, K., Zhang, J., Cheng, S., Heckscher, E., Talbot, W. S., and Schier, A. F. (1999). The EGF-CFC protein one-eyed pinhead is essential for nodal signaling. *Cell* **97,** 121–132.

Guger, K. A., and Gumbiner, B. M. (1995). β-Catenin has Wnt-like activity and mimics the Nieuwkoop signaling center in Xenopus dorsal–ventral patterning. *Dev. Biol.* **172,** 115–125.

Hammerschmidt, M., Pelegri, F., Mullins, M. C., Kane, D. A., Eeden, F.J.M. v., Granato, M., Brand, M., Furutani-Saki, M., Haffter, P., Heisenberg, C.-P., Jiang, Y.-J., Kelsh, R. N., Odenthal, J., Warga, R. M., and Nusslein-Volhard, C. (1996a). *dino* and *mercedes*, two genes regulating dorsal development in the zebrafish embryo. *Development* **123,** 95–102.

Hammerschmidt, M., Serbedzija, G. N., and McMahon, A. P. (1996b). Genetic analysis of dorsoventral pattern formation in the zebrafish: Requirement of a BMP-like ventralizing activity and its dorsal repressor. *Genes Dev.* **10,** 2452–2461.

Harland, R. M., and Gerhart, J. (1997). Formation and function of the Spemann organizer. *Annu. Rev. Cell Dev. Biol.* **13,** 611–667.

Joubin, K., and Stern, C. D. (1999). Molecular interactions continuously define the organizer during the cell movements of gastrulation. *Cell* **98,** 559–571.

Kelly, C., Chin, A. J., Leatherman, J. L., Kozlowski, D. J., and Weinberg, E. S. (2000). Maternally controlled β-catenin-mediated signaling is required for organizer formation in the zebrafish. *Development* **127,** 3899–3911.

Kelly, G. M., Erezyilmaz, D. F., and Moon, R. T. (1995). Induction of a secondary embryonic axis in zebrafish occurs following the overexpression of beta-catenin. *Mech. Dev.* **53,** 261–273.

Kishimoto, Y., Lee, K., Zon, L., Hammerschmidt, M., and Schulte-Merker, S. (1997). The molecular nature of zebrafish *swirl*: BMP2 function is essential during early dorsoventral patterning. *Development* **124,** 4457–4466.

Kodjabachian, L., Dawid, I. B., and Toyama, R. (1999). Gastrulation in zebrafish: What mutants teach us. *Dev. Biol.* **213,** 231–245.

Koos, D. S., and Ho, R. K. (1998). The nieuwkoid gene characterizes and mediates a Nieuwkoop-center-like activity in the zebrafish. *Curr. Biol.* **8,** 1199–1206.

Koos, D. S., and Ho, R. K. (1999). The nieuwkoid/dharma homeobox gene is essential for bmp2b repression in the zebrafish pregastrula. *Dev. Biol.* **215,** 190–207.

Krauss, S., Johansen, T., Korzh, V., and Fjose, A. (1991a). Expression of the zebrafish paired box gene pax[zf-b] during early neurogenesis. *Development* **113,** 1193–1206.

Krauss, S., Johansen, T., Korzh, V., and Fjose, A. (1991b). Expression pattern of zebrafish pax genes suggests a role in early brain regionalization. *Nature* **353,** 267–270.

Massagué, J. (1998). TGF-β signal transduction. *Annu. Rev. Biochem.* **67,** 753–791.

Moos, M., Wang, S., and Krinks, M. (1995). Anti-Dorsalizing Morphogenetic Protein is a novel TGF-β homolog expressed in the Spemann organizer. *Development* **121,** 4293–4301.

Mori, H., Miyazaki, Y., Morita, T., Nitta, H., and Mishina, M. (1994). Different spatio-temporal expressions of three otx homeoprotein transcripts during zebrafish embryogenesis. *Brain Res. Mol. Brain Res.* **27,** 221–231.

Müller, M. V., Weizsäcker, E., and Campos-Ortega, J. A. (1996). Transcription of a zebrafish gene of the hairy-Enhancer of split family delineates the midbrain anlage in the neural plate. *Dev. Genes Evol.* **206,** 153–160.

Mullins, M. C., Hammerschmidt, M., Kane, D. A., Odenthal, J., Brand, M., EEden, F.J.M. v., Furutani-Saki, M., Granato, M., Haffter, P., Heisenberg, C.-P., Jiang, Y.-J., Kelsh, R. N., and Nusslein-Volhard, C. (1996). Genes establishing dorsoventral pattern formation in the zebrafish embryo: The ventral specifying genes. *Development* **123,** 81–93.

Nasevicius, A., and Ekker, S. C. (2000). Effective targeted gene "knockdown" in zebrafish [In Process Citation]. *Nat. Genet.* **26,** 216–220.

Nguyen, V., Schmidt, B., Trout, J., Connors, S. A., Ekker, M., and Mullins, M. C. (1998). Ventral and lateral regions of the zebrafish gastrula, including neural crest progenitors, are established by a *bmp2b/swirl* pathways of genes. *Dev. Biol.* **199,** 93–100.

Nikaido, M., Tada, M., Saji, T., and Ueno, N. (1997). Conservation of BMP signaling in zebrafish mesoderm patterning. *Mech. Dev.* **61,** 75–88.

Nikaido, M., Tada, M., and Ueno, N. (1999). Restricted expression of the receptor serine/threonine kinase BMPR-IB in zebrafish. *Mech. Dev.* **82,** 219–222.

Odenthal, J., and Nusslein-Volhard, C. (1998). fork head domain genes in zebrafish. *Dev. Genes Evol.* **208,** 245–258.

Peyrieras, N., Lu, Y., Renucci, A., Lemarchandel, V., and Rosa, F. (1996). Inhibitory interactions controlling organizer activity in fish. *C. R. Acad. Sci. III* **319,** 1107–1112.

Peyrieras, N., Strahle, U., and Rosa, F. (1998). Conversion of zebrafish blastomeres to an endodermal fate by TGF-beta-related signaling. *Curr. Biol.* **8,** 783–786.

Piccolo, S., Sasai, Y., Lu, B., and De Robertis, E. M. (1996). Dorsoventral patterning in Xenopus: Inhibition of ventral signals by direct binding of chordin to BMP-4. *Cell* **86,** 589–598.

Postlethwait, J. H., Yan, Y. L., Gates, M. A., Horne, S., Amores, A., Brownlie, A., Donovan, A., Egan, E. S., Force, A., Gong, Z., Goutel, C., Fritz, A., Kelsh, R., Knapik, E., Liao, E., Paw, B.,

Ransom, D., Singer, A., Thomson, M., Abduljabbar, T. S., Yelick, P., Beier, D., Joly, J. S., Larhammar, D., Rosa, F., *et al.* (1998). Vertebrate genome evolution and the zebrafish gene map. *Nat. Genet.* **18,** 345–349.

Reilly, K. M., and Melton, D. A. (1996). Short-range signaling by candidate morphogens of the TGF beta family and evidence for a relay mechanism of induction. *Cell* **86,** 743–754.

Renucci, A., Lemarchandel, V., and Rosa, F. M. (1996). An activated form of type U serine/threonine kinase receptor TARAM-A reveals a specific signalling pathway invloved in fish head organizer formation. *Development* **122,** 3735–3743.

Rissi, M., Wittbrodt, J., Délot, E., Naegeli, M., and Rosa, F. M. (1995). Zebrafish *radar*: A new member of the TGF-β family defines dorsal regions of the neural plate and the embryonic retina. *Mech. Dev.* **49,** 223–234.

Schier, A. F., and Shen, M. M. (2000). Nodal signalling in vertebrate development [In Process Citation]. *Nature* **403,** 385–389.

Schier, A. F., and Talbot, W. S. (1998). The zebrafish organizer. *Curr. Opin. Genet. Dev.* **8,** 464–471.

Schmid, B., Furthauer, M., Connors, S. A., Trout, J., Thisse, B., Thisse, C., and Mullins, M. C. (2000). Equivalent genetic roles for bmp7/snailhouse and bmp2b/swirl in dorsoventral pattern formation. *Development* **127,** 957–967.

Schneider, S., Steinbeisser, H., Warga, R. M., and Hausen, P. (1996). Beta-catenin translocation into nuclei demarcates the dorsalizing centers in frog and fish embryos. *Mech. Dev.* **57,** 191–198.

Schulte-Merker, S., Lee, K. J., McMahon, A. P., and Hammerschmidt, M. (1997). The zebrafish organizer requires chordino [letter]. *Nature* **387,** 862–863.

Schulte-Merker, S., van Eeden, F. J., Halpern, M. E., Kimmel, C. B., and Nusslein-Volhard, C. (1994). no tail (ntl) is the zebrafish homologue of the mouse T (Brachyury) gene. *Development* **120,** 1009–1015.

Talbot, W. S., Trevarrow, B., Halpern, M. E., Melby, A. E., Farr, G., Postlethwait, J. H., Jowett, T., Kimmel, C. B., and Kimelman, D. (1995). A homeobox gene essential for zebrafish notochord development. *Nature* **378,** 150–157.

Thisse, C., and Thisse, B. (1999). Antivin, a novel and divergent member of the TGFbeta superfamily, negatively regulates mesoderm induction. *Development* **126,** 229–240.

Thisse, C., Thisse, B., Halpern, M. E., and Postlethwait, J. H. (1994). *goosecoid* expression in neurectoderm and mesendoderm is disrupted in zebrafish *cyclops* gastrulas. *Dev. Biol.* **164,** 420–429.

Weinberg, E. S., Allende, M. L., Kelly, C. S., Abdelhamid, A., Murakami, T., Andermann, P., Doerre, O. G., Grunwald, D. J., and Riggleman, B. (1996). Developmental regulation of zebrafish MyoD in wild-type, no tail and spadetail embryos. *Development* **122,** 271–280.

Wittbrodt, J., and Rosa, J. M. (1994). Disruption of mesoderm and axis formation in fish by ectopic expression of activins variants: The role of maternal activin. *Genes Dev.* **8,** 1448–1462.

Yamanaka, Y., Mizuno, T., Sasai, Y., Kishi, M., Takeda, H., Kim, C. H., Hibi, M., and Hirano, T. (1998). A novel homeobox gene, dharma, can induce the organizer in a non-cell-autonomous manner. *Genes Dev.* **12,** 2345–2353.

Yeo, C., and Whitman, M. (2001). Nodal signals to Smads through Cripto-dependent and Cripto-independent mechanisms. *Mol. Cell* **7,** 949–957.

Zimmerman, L. B., De Jesus-Escobar, J. M., and Harland, R. M. (1996). The Spemann organizer signal noggin binds and inactivates bone morphogenetic protein 4. *Cell* **86,** 599–606.

Received for publication March 15, 2001
Revised August 27, 2001
Accepted October 1, 2001
Published online November 28, 2001